AMERICAN JOURNAL OF PHYSIOLOGY
CELL PHYSIOLOGY

*Am J Physiol Cell Physiol* 323: C69–C83, 2022.
*First published May 25, 2022; doi:10.1152/ajpcell.00455.2021*

REVIEW

*Mathematical Modeling of Cellular Processes*

# Mechanisms and mathematical modeling of ROS production by the mitochondrial electron transport chain

**Sandeep Chenna,[1] Werner J. H. Koopman,[2,3]* Jochen H. M. Prehn,[1,4] and Niamh M. C. Connolly[1]***

[1]*Department of Physiology and Medical Physics, Centre for Systems Medicine, Royal College of Surgeons in Ireland, Dublin, Ireland;* [2]*Department of Pediatrics, Amalia Children's Hospital, Radboud Institute for Molecular Life Sciences, Radboud Center for Mitochondrial Disorders, Radboud University Medical Center, Nijmegen, The Netherlands;* [3]*Human and Animal Physiology, Wageningen University, Wageningen, The Netherlands; and* [4]*SFI FutureNeuro Research Centre, Dublin, Ireland*

## Abstract

Reactive oxygen species (ROS) are recognized both as damaging molecules and intracellular signaling entities. In addition to its role in ATP generation, the mitochondrial electron transport chain (ETC) constitutes a relevant source of mitochondrial ROS, in particular during pathological conditions. Mitochondrial ROS homeostasis depends on species- and site-dependent ROS production, their bioreactivity, diffusion, and scavenging. However, our quantitative understanding of mitochondrial ROS homeostasis has thus far been hampered by technical limitations, including a lack of truly site- and/or ROS-specific reporter molecules. In this context, the use of computational models is of great value to complement and interpret empirical data, as well as to predict variables that are difficult to assess experimentally. During the past decades, various mechanistic models of ETC-mediated ROS production have been developed. Although these often-complex models have generated novel insights, their parameterization, analysis, and integration with other computational models are not straightforward. In contrast, phenomenological (sometimes termed "minimal") models use a relatively small set of equations to describe empirical relationship(s) between ROS-related and other parameters and generally aim to explore system behavior and generate hypotheses for experimental validation. In this review, we first discuss ETC-linked ROS homeostasis and introduce various detailed mechanistic models. Next, we present how bioenergetic parameters (e.g., NADH/$NAD^+$ ratio and mitochondrial membrane potential) relate to site-specific ROS production within the ETC and how these relationships can be used to design minimal models of ROS homeostasis. Finally, we illustrate how minimal models have been applied to explore pathophysiological aspects of ROS.

*electron transport chain; mathematical model; mitochondria; reactive oxygen species*

## INTRODUCTION

Reactive oxygen species (ROS) are (sometimes highly) reactive molecules produced throughout the cell upon partial reduction (gain of electrons) of molecular oxygen ($O_2$). Through their mediation of reduction-oxidation (redox)-dependent bioreactions, ROS play a central role in redox-dependent cellular processes such as cell adaptation and metabolic regulation, and in the fine-tuning of molecular pathways such as AMP-activated protein kinase (AMPK) and hypoxia-inducible factor (HIF) signaling (1–3). In addition to signaling, excessive or sustained elevated ROS levels can induce oxidative stress (4). This stress, often paralleled by alterations in redox state, is a key contributing factor in the pathomechanism of many human diseases (3, 5, 6). To prevent undesired changes in redox state and ROS levels, ROS are tightly controlled by the action of various scavenging mechanisms including enzymatic antioxidants such as superoxide dismutases (SOD), glutathione peroxidases (GPx), or thioredoxins (TRx), and nonenzymatic antioxidants like vitamin C, vitamin E, and glutathione (GSH) (7).

### Cellular Sites of ROS Generation

ROS can be produced at various sites within the cell (Fig. 1; 3, 12, 13), including peroxisomes (e.g., xanthine oxidases, acyl-CoA oxidases), the endoplasmic reticulum (ER)/microsomes (e.g., NADH oxidase, cytochrome P450), the plasma membrane (e.g., NAD(P)H oxidases, lipoxygenases), and mitochondria [e.g., electron transport chain (ETC) complexes, dehydrogenases]. Although other sources of ROS should not be neglected (13, 14), mitochondria-generated ROS have been shown to play an important role in both cell signaling and damaging events, in particular during pathological

*W. J. H. Koopman and N. M. C. Connolly contributed equally to this work.
Correspondence: W. J. H. Koopman (werner.koopman@radboudumc.nl); N. M. C. Connolly (niamhmconnolly@rcsi.ie).
Submitted 22 December 2021 / Revised 12 May 2022 / Accepted 23 May 2022

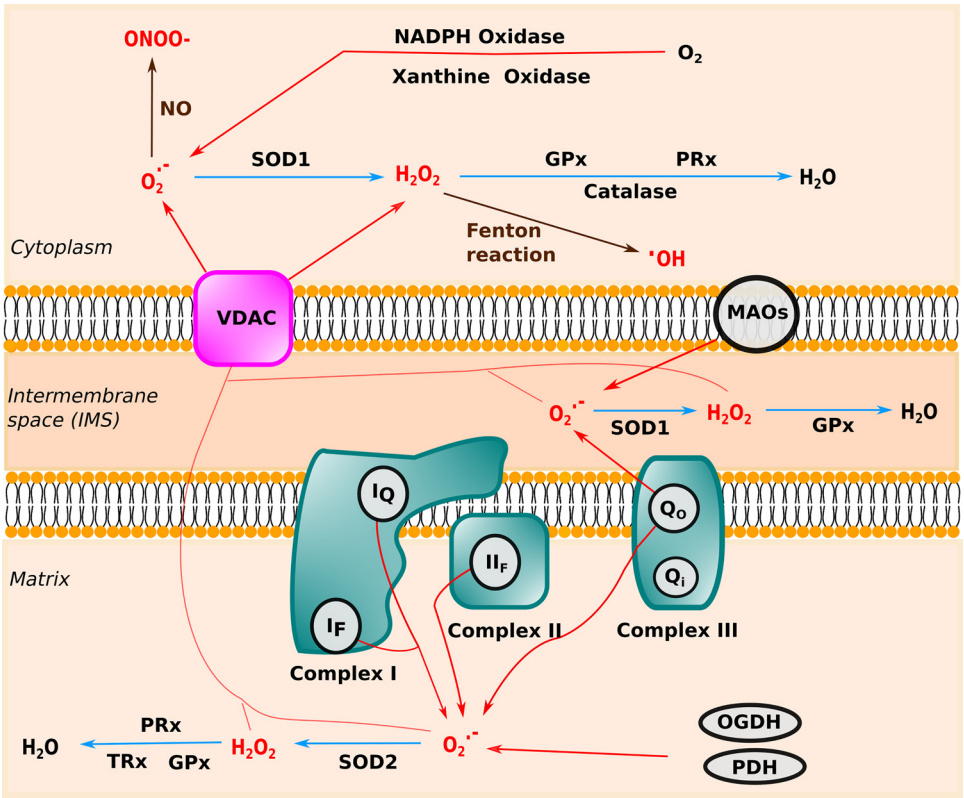


**Figure 1.** Production, transport, and metabolism of mitochondrial reactive oxygen species. Reactive oxygen species (ROS, red) are generated in various cellular compartments including mitochondria and the cytoplasm. The predominant sources of ROS are indicated. Some sources may directly generate $H_2O_2$ (8). Scavenging reactions (blue arrows) subsequently reduce superoxide ($O_2^{\cdot-}$) to hydrogen peroxide ($H_2O_2$) and water ($H_2O$). Alternative reactions (brown arrows) can lead to formation of toxic compounds like peroxynitrite ($ONOO^-$) and hydroxyl radicals (·OH). Since $H_2O_2$ is membrane-permeable, it can freely diffuse through the mitochondrial membranes (9, 10). Alternatively, ROS can be conveyed across the mitochondrial outer membrane by voltage-dependent anion channels (VDACs) (11). See main text for further details. GPx, glutathione peroxidase; $I_F$, flavomononucleotide/flavin site of CI; MAO, monoamine oxidase; NO, nitric oxide; OGDH, 2-oxoglutarate dehydrogenase (a.k.a. α-ketoglutarate dehydrogenase); PDH, pyruvate dehydrogenase; PRx, peroxiredoxins; SOD, superoxide dismutase; TRx, thioredoxin.

conditions (15–18). Within mitochondria, several ROS-producing sites have been identified. These include tricarboxylic acid (TCA) cycle enzymes (e.g., 2-oxoglutarate dehydrogenase), monoamine oxidases (MAOs), 2-oxoacid dehydrogenase complexes (OADHC), mitochondrial *sn*-glycerol-3-phosphate dehydrogenase (mGPDH), dihydroorotate dehydrogenase (DHDOH), the electron transferring flavoprotein (ETF/ETF:QOR system), and multiple sites within the ETC (8, 19). Importantly, mitochondria can also remove ROS and thereby serve as (local) ROS "sinks" (20–22). Here, we primarily focus on ETC-derived ROS (see ROS PRODUCTION BY THE ELECTRON TRANSPORT CHAIN).

## Types of ROS and Their Removal

The superoxide anion ($O_2^{\cdot-}$) is generally considered the primary ROS and is formed upon single-electron reduction of $O_2$ (Fig. 1). $O_2^{\cdot-}$ can be converted into hydrogen peroxide ($H_2O_2$) by spontaneous dismutation or through a SOD-catalyzed enzymatic reaction (23–25). Various SOD isoforms exist including *1*) manganese SOD (i.e., SOD2), primarily expressed in the mitochondrial matrix and *2*) copper-zinc (CuZn) SOD (i.e., SOD1), primarily expressed in the cytosol and mitochondrial intermembrane space (IMS) between the mitochondrial inner (MIM) and outer membranes (MOM). Alternatively, $O_2^{\cdot-}$ can react with nitric oxide (NO) to generate peroxynitrite ($ONOO^-$), a potentially toxic reactive nitrogen species (16). $H_2O_2$ can serve as a substrate for the Fenton reaction (26), in which it gains another electron by reacting with ferrous iron ($Fe^{2+}$) to yield hydroxyl ions ($OH^-$) and highly reactive hydroxyl radicals (·OH). $H_2O_2$ can also be reduced to water ($H_2O$) by the action of catalase (CAT; peroxisomes and cytoplasm), peroxiredoxins (PRx; predominantly in the cytoplasm), GPx [via GSH oxidation into glutathione disulfide (GSSG)], or TRx (primarily in the mitochondrial matrix). In the remainder of this review, we will use the term "ROS" to represent both $O_2^{\cdot-}$ or $H_2O_2$, and distinguish between these molecules when appropriate.

## Quantification of ROS

Quantitative methods (e.g., spectroscopy) can provide absolute ROS concentrations. In contrast, semiquantitative methods deliver indirect and/or relative readouts of changes in ROS level, for instance by quantifying the fluorescence signal of a chemical or proteinaceous reporter molecule, or the activity of a redox-sensitive enzyme. Numerous experimental strategies have been provided to assess extracellular and (sub)cellular ROS levels (27–34). These include enzyme inhibition assays (e.g., aconitase activity), electron paramagnetic resonance spectroscopy, and fluorescent/bioluminescent chemical (e.g., hydroethidine/lucigenin) or protein-based (e.g., HyPer) reporter molecules (30, 35–39). However, cellular ROS and derived species are often produced locally and display metabolism-, time- and species-dependent removal, reactivity, and diffusivity (40–44). These phenomena, in combination with the complex cellular reaction environment and general lack of truly ROS-specific reporter molecules, make quantitative detection and manipulation of ROS challenging (8, 45, 46). However, ongoing reporter optimization is improving this situation (see Refs. 22 and 47), provided that experiments are correctly implemented, interpreted, and compared between studies. Furthermore, optogenetic techniques for selective spatiotemporal ROS generation are available, for example, see Refs. (48 and 49). Comparison

of experimental results between studies is further complicated due to the use of different energy substrates, measurement techniques, and biological models. For instance, it is challenging to compare data obtained with isolated mitochondria lacking cytosolic antioxidants (but allowing tight external control of substrate availability) with live cell analysis of intracellular mitochondria. In this context, the use of computational models is of significant value to complement and interpret experiments, as well as to predict (changes in) variables that are difficult to assess experimentally.

### Mathematical Modeling of ROS Homeostasis

Computational models have been widely applied for mathematical representation and simulation of complex biological systems (see Refs. 50–58). This modeling enables analysis of the theoretical underpinnings of a system, investigation of its equilibrium properties and time-dependent behavior, and prediction of system characteristics under defined (experimental) constraints. Mathematical models can be applied to address some of the shortcomings associated with experimental ROS quantification, by providing a strategy to study those aspects of ROS and redox homeostasis that cannot be assessed by empirical means. In this sense, several models with a relatively high level of mechanistic detail and complexity have been developed, describing various aspects of ROS homeostasis such as production, scavenging, and signaling. Detailed models, however, tend to have a narrow scope as they necessarily describe a smaller number of unique components in great depth. The use of phenomenological equations with less mechanistic detail ("minimal models") is therefore useful for simulating system behavior in (patho)physiology, although such models require careful equation design that is directly based on the to-be-simulated condition or experiment.

A comprehensive guide for newcomers to the field of computational modeling and ROS metabolism was recently presented elsewhere (59). Therefore, we here focus on the mechanistic aspects of ETC-mediated ROS production (see ROS PRODUCTION BY THE ELECTRON TRANSPORT CHAIN), introduce several detailed models of ROS homeostasis (see DETAILED MATHEMATICAL MODELS OF MITOCHONDRIAL ROS HOMEOSTASIS, Table 1), outline how the relationships between relevant bioenergetic parameters and ETC-mediated ROS production can be utilized to develop minimal models (see RELEVANCE OF BIOENERGETIC AND OTHER PARAMETERS FOR PHENOMENOLOGICAL MODELS OF ROS PRODUCTION), and describe how such models can enhance our understanding of ROS homeostasis in disease pathology (see APPLYING PHENOMENOLOGICAL MODELS TO EXPLORE ROS-LINKED (PATHO)MECHANISMS).

## ROS PRODUCTION BY THE ELECTRON TRANSPORT CHAIN

The mitochondrial electron transport chain (ETC), or respiratory chain, consists of four multisubunit protein complexes (CI, CII, CIII, and CIV) that are embedded in the mitochondrial inner membrane (MIM). The ETC, together with the $F_1F_0$-ATP synthase, constitutes the ATP-generating mitochondrial oxidative phosphorylation (OXPHOS) system. With the exception of CII, all OXPHOS complexes are composed of subunits encoded by both nuclear DNA (nDNA) and mitochondrial DNA (mtDNA) (86). ETC complexes can form "supercomplexes" in various stoichiometries that are suggested to play a role in ETC complex function, assembly, and/or stabilization (87).

Functionally, the ETC sustains a trans-MIM proton-motive force (PMF), which consists of an electrical ($\Delta\psi_m$) and chemical ($\Delta$pH) component (see Ref. 88 and references therein). PMF formation entails the donation of electrons by NADH (at CI) and $FADH_2$ (at CII), followed by transport of these electrons by two electron carriers [ubiquinone (Q) and cytochrome-*c* (cyt-*c*)] to CIII and CIV, respectively. At CIV, electrons are donated to $O_2$ to form water ($H_2O$). The energy released by the transport of electrons is utilized to expel protons ($H^+$) from the mitochondrial matrix across the MIM (at CI, CIII, and CIV) into the intermembrane space (IMS). This yields an electrical gradient across the MIM entailing an inside-negative mitochondrial membrane potential ($\Delta\psi_m$) and elevated (more basic) matrix pH ($\Delta$pH). The PMF drives $F_1F_0$-ATP synthase-mediated ATP production by allowing the controlled backflow of $H^+$ into the mitochondrial matrix (89).

As ETC function involves electron transport and redox reactions, unintended electron escape can induce formation of $O_2^{\cdot-}$, $H_2O_2$, and other downstream ROS-related molecules (Fig. 1) (12, 19, 90). The precise location and amount of ETC-mediated ROS generation depend on many factors, including the mitochondrial substrate, $O_2$ concentration, rate of ATP synthesis, and ETC supercomplex levels (91, 92). ROS production by CII is mediated by its flavin site (IIf) and occurs primarily when CI and CIII are inhibited (8, 61, 93, 94). Although the significance of CII to overall mitochondrial ROS is still poorly understood, accumulating evidence suggests that CII-mediated ROS production is relevant during conditions of ischemia/reperfusion (61, 95) and inflammation (96). Although it appears that CIV is not directly involved in ROS production, its inhibition/mutation alters electron flow through upstream ETC complexes and thereby affects ROS production from these sites (97). In this review, we primarily focus on CI and CIII as these complexes appear to be the primary ETC-sites for ROS production (8, 42).

### ROS Production by Complex I

Complex I (CI) [i.e., NADH:ubiquinone oxidoreductase or NADH dehydrogenase (EC 1.6.5.3)] is the largest enzyme of the ETC (~1 MDa) consisting of 44 different subunits (98). CI catalyzes the oxidation of NADH to $NAD^+$ and reduction of ubiquinone (Q) to ubiquinol ($QH_2$). This redox reaction involves the transfer of two electrons and translocation of $4H^+$ from the matrix into the IMS:

$$NADH + 2H^+ + Q + 4H^+_{(matrix)} \rightleftarrows NAD^+ + QH_2 + 4H^+_{(IMS)} \quad (1)$$

Electron transfer from NADH to Q is mediated by the flavin mononucleotide (FMN) group and a series of iron-sulfur (FeS) clusters (N1–N6; Fig. 2). This transfer occurs from lower to higher redox potentials in the order: NADH→FMN→N3→N1b→N4→N5→N6a→N6b→N2→Q (90, 99–101)). Due to their location within CI, the FeS clusters are relatively

**Table 1.** *Selected mechanistic models of ETC-mediated ROS homeostasis*

| Biological Model(s) | Reactions Included | Model Type | Used Code | Conclusions | References |
|---|---|---|---|---|---|
| | | | *Models of individual ETC complexes* | | |
| Isolated bovine heart mitochondria | CI | Kinetic | MATLAB | $FMNH^-$ ($I_F$) and semiquinone ($I_Q$) are the primary CI ROS sources. The $I_F$ site produces the majority of ROS, although $I_Q$ plays a major role in RET conditions. A decrease in NAD(H) pool size increases ROS levels and the excess ROS originates from the $I_F$ site. | (60) |
| Mammalian heart isolated mitochondria, isolated enzyme | CII | Kinetic | MATLAB | The primary ROS produced from CII is superoxide. | (61) |
| Literature-based, generic (no tissue specificity) | CII | Kinetic | DBSolve Optimum[%] | Increase in ROS production upon inhibition of CIII or CII (Q binding site), or disintegration of CII, is because of suppression of SQR activity, which changes the dependency of ROS production on succinate concentration. | (62) |
| Isolated rat brain mitochondria | CIII | Rule-based | Not specified | CIII ROS production exhibits bistabilty: anoxia causes a switch from a low to high ROS production state, and the high state of ROS production remains even after returning to normoxia. | (63) |
| Literature-based, generic (no tissue specificity) | CIII + AA | Kinetic | Mathematica | Cyt $b_{566}$ and Cyt $b_{562}$ redox states can be used to predict superoxide production from antimycin inhibited $Q_O$ site. | (64) |
| Literature-based, generic (no tissue specificity) | CIII + pH + PMF + AA | Kinetic | MATLAB | A functional dimer hypothesis was not required to explain experimental datasets used for parameterising the model. The model exhibits bistability (different ROS for same $\Delta\psi_m$). Redox specific binding at the $Q_i$ site is thermodynamically infeasible. | (65) |
| Literature-based, generic (no tissue specificity) | CIII + Q + Cyt-c + pH + $\Delta\psi_m$ + AA | Kinetic | Not specified | CIII ROS production is dependent on quinone pool reduction and $\Delta\psi_m$. The $\Delta\psi_m$ dependency is exponential and when inhibited by antimycin A, ROS production is independent of $\Delta\psi_m$. | (66) |
| | | | *Models of multiple ETC complexes* | | |
| Isolated rat brain mitochondria, succinate, pyruvate/malate | CI + CIII + FET + RET + TCA + NS | Rule-based | C++ | The whole RC exhibits bistability (67). A further simplified model (68) was used to show existence of multiple RC steady states and how the interaction of these multiple RC steady states with TCA cycle, mediated by NADH, leads to ROS and $\Delta\psi_m$ oscillations. | (67, 68) |
| Cardiomyocytes | CI + CIII + FET + RET + MS | Kinetic | MATLAB | Oxidizing mitochondrial conditions initially decrease ROS production as $\Delta\psi_m$ decreases and the NAD pool is oxidized, but any further increase causes an increase in ROS as GSH becomes oxidized. | (69) Submodels based on (70) (CI), (71) and (72) (CII, CIII, CIV). |
| Literature-based, generic (no tissue specificity) | CI + CIII + pH + $\Delta\psi_m$ + I + MS | Kinetic | DBSolve Optimum[%] | Semiquinone ($I_Q$) should be considered as an additional CI ROS site. Inhibiting CIII and CIV increases ROS production from this site. | (73) |
| Cardiomyocytes + ischemia | CI + CIII + FET + RET + $O_2^{\cdot-}$ + $H_2O_2$ + SOD | Kinetic | MATLAB | $P_i$ activation of CIII is due to an increase in Q pool reduction. ROS contribution from CIII is higher than from CI in physiological conditions. This model was further extended to include CII (74) and showed that CII and CIII contribute to basal ROS levels and that CI ROS becomes significant under pathological conditions. | (75) (74) |

*Continued*

**Table 1.—** *Continued*

| Biological Model(s) | Reactions Included | Model Type | Used Code | Conclusions | References |
|---|---|---|---|---|---|
| | | | *Models of ROS scavenging* | | |
| Cardiomyocytes | GPx + CAT + TRx + PRx + MCS + MRC | Kinetic | MATLAB | This model (76) reported lower ROS levels than previous models (nM to pM ranges for both $H_2O_2$ and $O_2^{\cdot-}$). They showed that compartmentalization plays a significant role in controlling ROS levels, the RE and overall system dynamics, and that this is mediated by exchange of redox species. The model is based on Refs. 77 and 78) and was used to characterize mitochondrial oscillations (77) and ROS-induced ROS release, to show that both Trx and GPx systems are required for maintaining minimal ROS levels (78), and to show that mitochondria exhibit chaotic (non-periodic) dynamics in oxidative stress conditions (79) | (76) (77) (78) (80) (79) |
| Liver | GR | Kinetic | Not specified | GR operates in alternate ping pong and sequential pathways depending on GSSG and $NADP^+$ concentrations. | (81) |

$\Delta\psi_m$, mitochondrial membrane potential; AA, antimycin a inhibition; CAT, catalase; CI, complex I; CIII, complex III; cyt-*c*, cytochrome-*c*; ETC, electron transport chain; FET, forward electron transfer; GPx, glutathione peroxidase; GR, glutathione reductase; GSSG, glutathione disulfide; $H_2O_2$, hydrogen peroxide; I, various inhibitors; $I_F$, flavomononucleotide/flavin site of CI; $I_Q$, semiquinone Q binding site of CI; MS, minimal ROS scavenging included; MCS, mitochondrial and cytosolic ROS scavenging; MRC, main redox couples; MT, multiple tissues; NS, no ROS scavenging included; $O_2^{\cdot-}$, superoxide; pH, pH-dependency included; $P_i$, inorganic phosphate; PMF, proton-motive force dependency included; PRx, peroxiredoxins; Q, quinone pool; RC, respiratory chain; RE, redox environment; RET, reverse electron transfer; ROS, reactive oxygen species; SQR, succinate-Q reductase, SOD, superoxide dismutase; TCA, tricarboxylic acid cycle; TRx, thioredoxins.

[%]DBSolve Optimum software (82).

Model Types—Kinetic: These models represent mechanisms involved in a biological process/system as sets of reactions. They are defined by its network with components and their stoichiometry, rate equations, initial conditions, and other environmental constraints (83). They can be detailed and high dimensional with a lot of reactions or minimal. All the models in the table are deterministic. But there are some models which do consider the processes involved in ROS production as probabilistic events and apply stochastic approaches (84, 85). Rule based: These models are constructed automatically based on a rule set and may or may not represent mechanistic details of the biological process.

Code availability:

Ref. 60: full equations and variables are provided, code not provided;
Ref. 61: https://www.jbc.org/cms/10.1074/jbc.RA120.014483/attachment/44212d6e-a0e7-4190-92ee-83ed6b14cd43/mmc1.zip.
Ref. 62: full equations and variables are provided, code not provided; (SBML file link not provided)
Ref. 63: full equations and variables are provided, code not provided;
Ref. 64: full equations and variables are provided, code not provided;
Ref. 65: full equations and variables are provided, code not provided;
Ref. 66: full equations and variables are provided, code not provided;
Ref. 67: http://www.bq.ub.es/bioqint/ros_model/plcb2010.cpp.tar.gz.
Ref. 69: https://icm.jhu.edu/models/.
Ref. 70: full equations and variables are provided, code not provided;
Ref. 71: full equations and variables are provided, code not provided;
Ref. 72: full equations and variables are provided, code not provided;
Ref. 73: full equations and variables are provided, code not provided;
Ref. 75: https://www.ncbi.nlm.nih.gov/labs/pmc/articles/PMC4776027/bin/mmc1.pdf.
Ref. 76: http://gforge.icm.jhu.edu/gf/projects/mitochondrial_energetics_redox/.
Ref. 77: full equations and variables are provided, code not provided;
Ref. 78: full equations and variables are provided, code not provided;
Ref. 81: full equations and variables are provided, code not provided;

inaccessible to $O_2$ (16). It appears that CI-mediated ROS can originate from three sites (Fig. 2; dotted red circles): *1*) the FMN/flavin site ($I_F$), *2*) the FeS cluster N2, and *3*) the Q binding site ($I_Q$; more accurately the binding site for semiquinone $Q^-$, the intermediate redox state). The $I_F$ site is likely the primary site of CI-mediated $O_2^{\cdot-}$ production, which is mediated by the flavin mononucleotide semiquinone ($FMNH^-$) radical (102):

$$FMNH^- + O_2 \rightleftarrows \mathrm{FMNH} + O_2^{\cdot-} \quad (2)$$

Pharmacological inhibitors and other electron carriers within CI can modulate $I_F$-mediated $O_2^{\cdot-}$ production by altering electron transfer through CI, which affects the $FMNH^-$ lifetime (102). For instance, the CI inhibitor rotenone binds within the Q-binding site of CI (103) (Fig. 2). This impairs electron transfer and thereby increases $O_2^{\cdot-}$ production at the $I_F$ site and other upstream enzymes [e.g., 2-oxoglutarate dehydrogenase (OGDH), pyruvate dehydrogenase (PDH)] (8, 102). The rate of CI-mediated ROS production is also affected (i.e., reduced) by the incorporation of CI into respiratory chain supercomplexes (104). During *state 3* conditions (i.e., when mitochondria are actively producing ATP), a low NADH/$NAD^+$ ratio is maintained by electron transfer through the entire ETC to enable $F_1F_0$-ATP

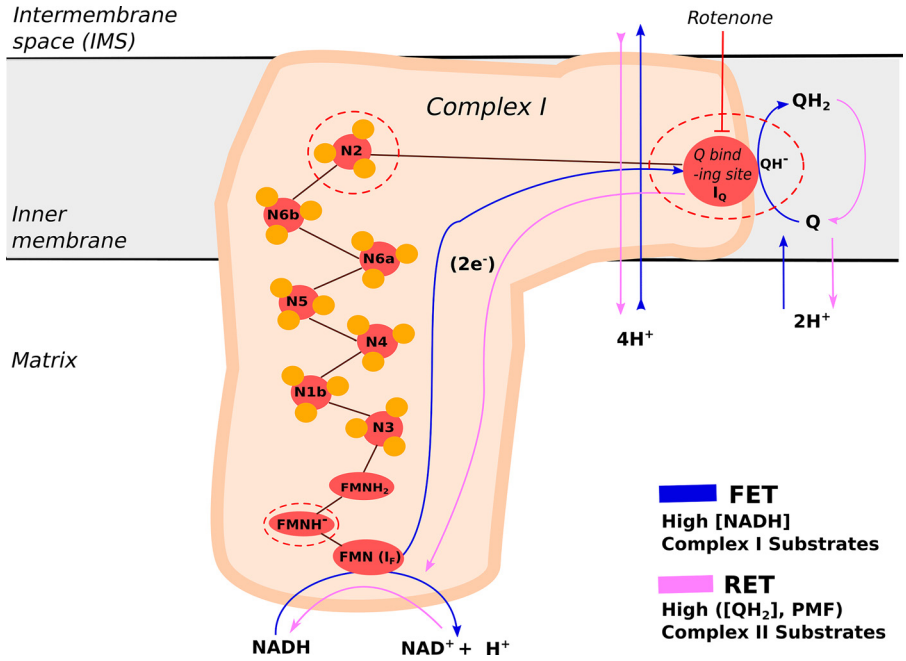


**Figure 2.** Electron transport reactions in complex I (CI) and potential reactive oxygen species (ROS) production sites. Electrons are transported from NADH via flavin mono nucleotide (FMN) and iron sulfur (Fe-S) clusters (yellow circles) to their final acceptor ubiquinone (Q). In CI, electron transport normally occurs in the "forward mode" (forward electron transport, FET; blue arrows). Under certain conditions, electron transport can also occur in "reverse mode" (reverse electron transport, RET; pink arrows). See main text for further details. PMF, proton-motive force; Q, ubiquinone form of coenzyme Q10; $QH_2$, ubiquinol form of coenzyme Q10.

synthase-mediated ATP production, and CI-mediated ROS production is relatively low (105). However, when increased NADH levels are not matched by increased electron transfer (e.g., during ETC dysfunction or apoptosis-linked cyt-*c* release), the rate of $I_F$-mediated $O_2^{\cdot-}$ production increases (16). Under these conditions, the $I_F$-site appears to constitute a main ROS source (15, 16, 61, 91).

In addition to its normal and most common "forward mode" of electron transfer (106), CI also can operate in "reverse mode" (18, 107, 108). These modes are characterized by forward electron transport (FET; Fig. 2, blue lines) and reverse electron transport (RET; Fig. 2, pink lines). RET is a thermodynamically unfavorable process, which occurs when electrons are transported from $QH_2$ back into CI, and leads to the consumption of $NAD^+$ and formation of NADH (15, 108). RET can occur for instance when electrons are delivered from CII to $QH_2$ during excessive oxidation of succinate or fatty acids (16, 18, 109). RET is facilitated during conditions of *1*) mitochondrial matrix ATP hydrolysis (i.e., when the $F_1F_0$-ATP synthase and ATP/ADP exchanging adenine nucleotide translocator (ANT) operate in reverse), *2*) *state 4* respiration (high ATP/ADP ratio and no ATP production), *3*) a highly negative (hyperpolarized) $\Delta\psi_m$, or *4*) a reduced Q pool. Although mitochondrial ROS production increases during RET, the source of this ROS is still not fully understood. Interestingly, ROS generation during RET is substantially inhibited by rotenone, likely via prevention of electron transfer to IQ and $I_F$ (15, 92, 105, 110, 111). This suggests that CI plays a central role in ROS production during RET. ROS production rates during RET are significantly higher than during FET (16, 92). The succinate levels required for stimulation of CII-mediated RET in experiments with isolated mitochondria are several folds higher than those observed during physiological conditions in living cells (91). However, it has been hypothesized that RET-linked ROS production is functionally relevant (111, 112) and experimental evidence demonstrated that RET can underlie CI-mediated ROS production during ischemia reperfusion (18).

## ROS Production by Complex III

Complex III (CIII) or Ubiquinol-cytochrome-c oxidoreductase (i.e., Cytochrome bc1 complex; EC 1.10.2.2) is a symmetrical dimeric complex, with each dimer consisting of 11 subunits (~240 kDa). CIII transfers electrons from $QH_2$ to cyt-*c* by means of the so-called "Q-cycle," in which oxidation of $QH_2$ to Q and reduction of two cyt-*c* molecules are coupled to the translocation of $4H^+$ from the matrix to the IMS (113):

$$QH_2 + 2\ Cyt\ c(Fe^{3+}) + 2H^+_{(matrix)} \rightleftarrows Q + 2\ Cyt\ c(Fe^{2+}) + 4H^+_{(IMS)} \quad (3)$$

The key redox carriers involved in the Q-cycle are the Rieske FeS protein (ISP), cytochrome $c_1$ (cyt-*c1*), cyt-*c*, and the cytochrome *b* hemes $b_L$ and $b_H$ (also known as $b_{566}$ and $b_{562}$, respectively) (114). Mechanistically, the complete process requires two cycles. In the first cycle (Fig. 3*A*), two electrons are released at the $Q_O$ site of CIII (also known as IIIQ) by $QH_2$ oxidation (Fig. 3, dashed red circle) and further conveyed through a high potential chain (Fig. 3, dotted green lines) and a low potential chain (Fig. 3, dotted blue lines). The end reaction of the high potential chain is reduction of cyt-*c* in an ISP- and cyt-*c1*-dependent manner. The low potential chain mediates the reduction of Q to $Q^-$ at the $Q_i$ site, mediated by $b_L$ and $b_H$. In the second cycle (Fig. 3*B*), oxidation of a second $QH_2$ at the $Q_O$ site results in the reduction of a second cyt-*c* via the high potential chain, and the reduction of $Q^-$ to $QH_2$ at the $Q_i$ site via the low-potential chain.

Previous experiments suggest that CIII-mediated $O_2^{\cdot-}$ generation occurs at the $Q_O$ site via a reaction between $QH_2$ and $O_2$ (specifically, the intermediate formation of an unstable semiquinone [$Q^-$] redox state), and that this $O_2^{\cdot-}$ is released into both the mitochondrial matrix and IMS (8). Alternatively, it has been proposed that $O_2^{\cdot-}$ is released

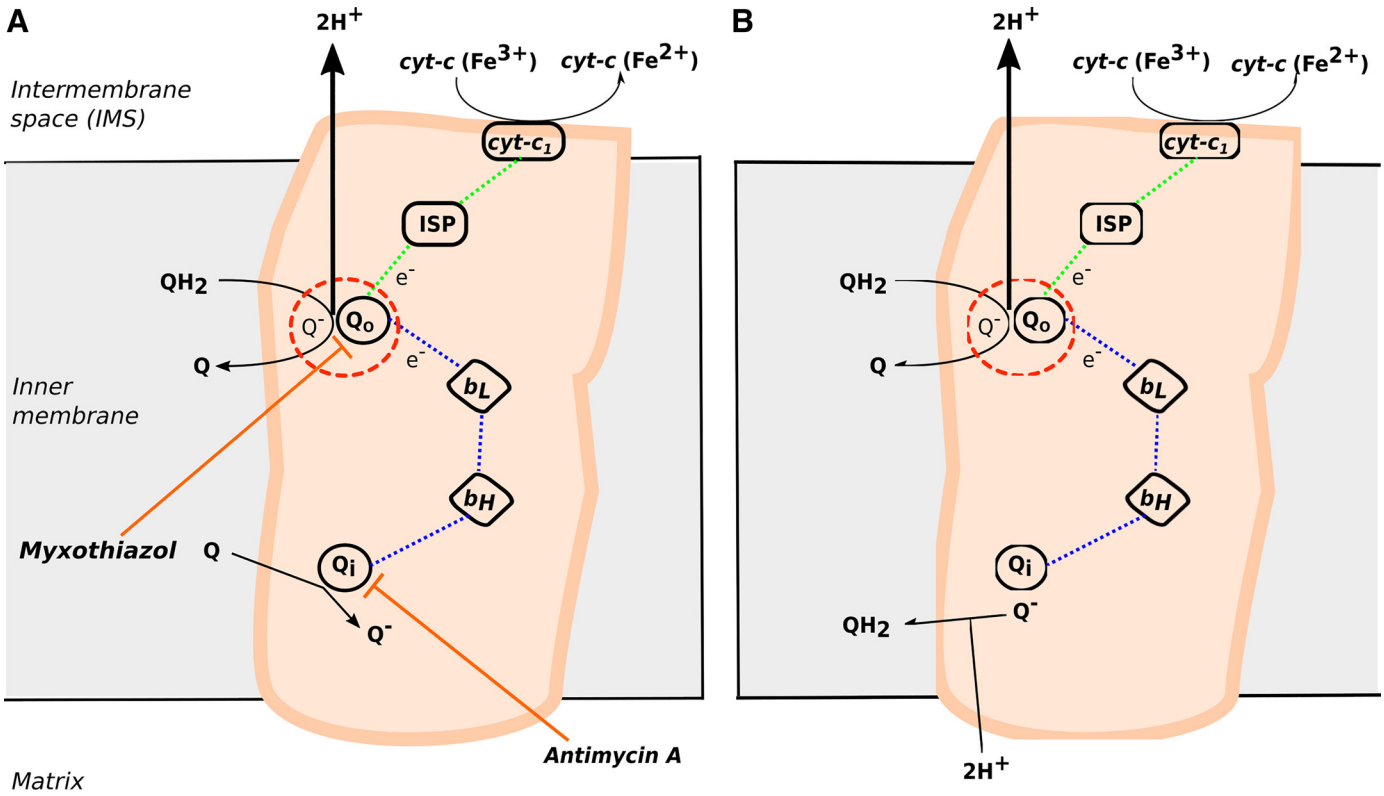


**Figure 3.** The Q-cycle in complex III (CIII) and potential reactive oxygen species (ROS) production sites. A complete Q-cycle involves the oxidation of two ubiquinol (ubiquinol form of CoQ10, $QH_2$) molecules at the $Q_O$ ROS producing site (red dashed circle), shown here as two cycles (*A* and *B*). The targets of CIII inhibitors are also shown. *A*: in the first cycle, two electrons are released at the $Q_O$ site by $QH_2$ oxidation (dotted red circle) and conveyed through high- (dotted green lines) and low- (dotted blue lines) potential chains. The high-potential chain reduces cyt-c in an iron-sulfur protein (ISP) and cytochrome $c_1$ (cyt-$c_1$)-dependent manner, whereas the low-potential chain mediates the reduction of ubiquinone form of coenzyme Q10 (Q) to $Q^{\cdot-}$ at the $Q_i$ site, mediated by $b_L$ and $b_H$. *B*: in the second cycle, oxidation of a second $QH_2$ at the $Q_O$ site results in the reduction of a second cyt-c via the high-potential chain, and the reduction of $Q^{\cdot-}$ to $QH_2$ at the $Q_i$ site via the low-potential chain. See main text for further details.

exclusively into the IMS (115). Although the maximal ROS production capacity of the $Q_O$ site exceeds that of all other ROS-producing sites in the ETC (8), it appears that $Q_O$-mediated $O_2^{\cdot-}$ generation is of lower magnitude than CI-mediated $O_2^{\cdot-}$ generation under physiological conditions (105, 116). However, when CI-mediated $O_2^{\cdot-}$ production is low, CIII-mediated $O_2^{\cdot-}$ production becomes more relevant (16, 61, 69, 75). Similar to CI, pharmacological inhibition of CIII can be applied to modulate ROS production. Application of antimycin A, which targets the $Q_i$ site (Fig. 3*A*) and thus inhibits $QH_2$ oxidation at the $Q_O$ site, strongly increases $O_2^{\cdot-}$ production by increasing $Q^{\cdot-}$ (113). In contrast, stigmatellin reduces $O_2^{\cdot-}$ production by preventing the transfer of the electron from the $Q_O$ site to ISP (15). Inhibition of $QH_2$ binding at the $Q_O$ site by myxothiazol generally decreases CIII-mediated $O_2^{\cdot-}$ production (Fig. 3*A*), although this inhibitor can also stimulate ROS production (117).

## DETAILED MATHEMATICAL MODELS OF MITOCHONDRIAL ROS HOMEOSTASIS

Various detailed computational models of ETC-linked ROS homeostasis have been reviewed previously (59, 118, 119). Several of these models are described in Table 1 focusing on ROS production by individual ETC complexes (*top*) or by multiple ETC complexes (*middle*), and ROS scavenging (*bottom*). These models not only delivered detailed information on complex-specific ROS production and antioxidant mechanisms, but also highlighted system characteristics such as oscillatory or bistable behavior (a bistable system can exist in two stable states e.g., high/low or on/off), and suggested mechanisms not observable by experimental analysis alone (Fig. 4). However, a complete mechanistic model of ETC-mediated ROS production is still lacking (119). Given their complexity, the calibration, implementation, and analysis of detailed computational models are far from straightforward. In this context, analysis of (more) phenomenological models can be highly rewarding. These models, which simulate system behavior using minimal equation sets, require careful equation design depending on the experimental system being simulated. This entails careful justification of the assumptions, exclusions, or simplifications used in the minimal model. For instance, many model parameter values are necessarily based on estimates, as they have not been measured empirically or are experimentally inaccessible. Therefore, the trade-off between model complexity and free/estimated parameters should be considered, as well as the trade-off between model simplification and the consequential loss of mechanistic insight (120). Models of specific experimental systems should be continually evaluated and validated in terms of their ability to provide mechanistic insight or predict the behavior of the system under

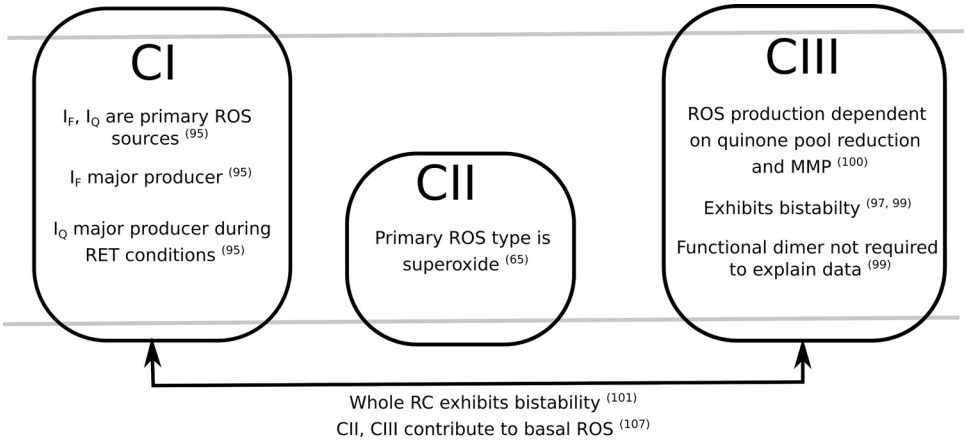


**Figure 4.** Findings obtained using computational models of reactive oxygen species (ROS) homeostasis. Further details on the model predictions are provided in the main text and Table 1. CI, mitochondrial complex I; CII, mitochondrial complex II; CIII, mitochondrial complex III; $I_F$, flavomononucleotide/flavin site of CI; $I_Q$, semiquinone Q binding site of CI; MMP, mitochondrial membrane potential (i.e. $\Delta\psi_m$); RC, respiratory chain; RET, reverse electron transport.

study while acknowledging that observations may not always be generalizable to other systems.

## RELEVANCE OF BIOENERGETIC AND OTHER PARAMETERS FOR PHENOMENOLOGICAL MODELS OF ROS PRODUCTION

Phenomenological models simulate empirical system behavior in relatively small equation sets, rather than explicitly describing detailed mechanisms. The aim of phenomenological models, therefore, is not to capture system behavior for an exhaustive number of conditions. For instance, a single phenomenological equation that adequately models ETC-mediated ROS production may not be directly informative regarding the underlying mechanism and/or the directionality of electron flow (e.g., RET vs. FET). Nevertheless, given their simplicity, ease of integration with other models, and ability to reproduce experiments under different conditions, phenomenological models have been successfully applied to investigate ROS homeostasis and continue to be a valuable resource (59, 77, 121, 122). For any mathematical model, careful consideration of equation design is vital. Since ETC-mediated ROS production is directly coupled to mitochondrial bioenergetics, parameters describing these bioenergetics are highly relevant for phenomenological equations. In this context, ROS production by the ETC primarily depends on the $NADH/NAD^+$ ratio, the $QH_2/Q$ ratio, the trans-MIM protonmotive force (PMF), $\Delta\psi_m$, and $O_2$ levels. The relevance of these parameters is explained in more detail in this section and an outline is provided about how these dependencies, along with ROS scavenging, can be incorporated into phenomenological equations of ETC-mediated ROS homeostasis.

### $NADH/NAD^+$ Ratio

Within mitochondria, $NAD^+$ is reduced to NADH in the TCA cycle. NADH, as a CI substrate, is oxidized back into $NAD^+$ by CI. These redox reactions, along with mitochondrial import of glycolysis-derived NADH, modulate the mitochondrial $NADH/NAD^+$ ratio, which plays an important role in cellular redox status (46). Moreover, this ratio affects the rate of ETC-mediated ROS production and other key processes including calcium homeostasis and gene expression (123). Within CI, the rate of ROS production at the $I_F$ site is determined by the concentrations of reduced/active flavin ($FMNH^-$) and $O_2$ (Eq. 2). The concentration of $FMNH^-$ itself is codetermined by the redox potential of $NAD^+$ ($E_{NAD+}$), among others (124). In addition, $FMNH^-$ only reacts with $O_2$ when the $FMNH^-$ binding site is free of nucleotides (125). Therefore, both the total pyridine nucleotide pool (NADtot = $NAD^+$ + NADH) and their ratios ($NADH/NAD^+$ or $NADH/NAD_{tot}$) directly impact the rate of $I_F$-mediated ROS production during FET (126, 127). This dependency has been experimentally observed in isolated and intact mitochondria during physiological conditions and in the presence of mitochondrial inhibitors (128–130).

Mathematically, the dependence of ETC-mediated ROS production on the $NADH/NAD^+$ ratio has been modeled using a square root function (Table 2) (121). However, it is not trivial to experimentally assess the quantitative relationship between the $NADH/NAD^+$ ratio and $I_F$-mediated ROS production, as ROS does not exclusively arise from the $I_F$ site, but also from other sites within the ETC (see ROS PRODUCTION BY THE ELECTRON TRANSPORT CHAIN). Experimental evidence (8, 131) suggests that $I_F$-mediated ROS production can be studied in isolation by inhibiting other ROS-generating sites like OGDH and PDH (using aspartate), and the $I_Q$ site (using rotenone). In one such study, an exponential nonlinear regression function (Table 2) was used to describe the experimental relationship between ROS production and the $NADH/NAD_{tot}$ ratio in isolated rat skeletal muscle mitochondria (92). In the case of RET, the quantitative relationship between ROS production and the $NADH/NAD^+$ ratio is still poorly understood. Using isolated rat skeletal muscle mitochondria, it was suggested that less than 10% of RET-mediated ROS production was sensitive to changes in the $NADH/NAD^+$ ratio (129). In addition to the $NADH/NAD^+$ ratio, RET-mediated ROS production by CI also depends on the PMF and the reduction state of the Q pool, with a reduced Q pool and $\Delta\psi_m$ hyperpolarization contributing to increased ROS (108). In this sense, it was proposed that the IQ site of CI may be a major ROS producer during RET (8). Given these uncertainties, it is still challenging to design meaningful phenomenological equation(s) that adequately describe CI-mediated ROS production during RET as a function of the $NADH/NAD^+$ ratio. Therefore, more detailed mathematical descriptions are currently better suited for this purpose.

**Table 2.** *Mathematical equations for phenomenological description of ETC-mediated ROS production*

| Function | Equation | Benefits | Limitations |
|---|---|---|---|
| Square root function | $\sqrt{\frac{NADH}{NAD^+}}$ | Generalized function, so insensitive to experimental data quality | Generalized functions may not give a good fit to training data<br>Function cannot be scaled/normalized |
| Exponential nonlinear regression function | $a.e^{\left(m.\frac{NADH_c}{NAD_{tot}}\right)} - c$ | Give a good fit to experimental training data<br>Function can be scaled/normalized | Sensitive to quality of experimental data<br>Parameters may not have biological interpretability |
| Hill function | $\frac{a^n.\Delta\Psi_m{}^n}{k^n+\Delta\Psi_m{}^n}$ | Parameters have biological interpretability<br>Function can be scaled/normalized | Sensitive to quality of experimental data |
| Boltzmann function | $\left(\frac{1}{1+e^{\left(\frac{\Delta\Psi_m-l}{k}\right)}}\right)$ | Parameters have biological interpretability<br>Applicable to any phenomenon exhibiting a threshold<br>Function is scaled/normalized | Sensitive to quality of experimental data |

ETC, electron transport chain; ROS, reactive oxygen species.

### $QH_2$/Q Ratio

$QH_2$ (reduced ubiquinol) and Q (oxidized ubiquinone) are established redox regulators of mitochondrial electron transport that also impact mitochondrial ROS production. The total quinone pool ($QH_2$ + Q) is directly upstream of CIII, through which it is connected with the cyt-*c* pool (Fig. 3) (132). CIII-mediated ROS production at the $Q_O$ site depends on the reduction state of cytochrome $b_L$ ($b_{566}$) (92), which closely mirrors the $QH_2$/Q ratio (8). This empirical relationship between $Q_O$-mediated ROS production and the extent of cytochrome $b_L$ reduction can be described by an exponential nonlinear regression function (Table 2) (92). Such functions were successfully applied to predict ROS production from both the $I_F$ and $Q_O$ site in the presence of various substrates/inhibitors (92).

### Proton Motive Force and Mitochondrial Membrane Potential ($\Delta\psi_m$)

The PMF arises from the trans-MIM proton electrochemical gradient consisting of $\Delta\psi_m$ and $\Delta$pH:

$$\mathrm{PMF(mV)} = \Delta\psi_m\mathrm{(mV)} - 60\ \Delta\mathrm{pH}\ \ (\mathrm{at}\ 25^\circ\mathrm{C}) \qquad (4)$$

The PMF is directly linked to mitochondrial ATP synthesis via the $F_1F_0$-ATPase and ADP/ATP exchange by the adenine nucleotide translocase (ANT) (133). Under most conditions, the magnitude of the PMF primarily depends on $\Delta\psi_m$ (89). Although changes in both $\Delta\psi_m$ and $\Delta$pH have been demonstrated to affect mitochondrial ROS production, $\Delta\psi_m$ is more extensively studied (91, 134). Here it is worth noting that experimental ROS detection using cationic fluorescent ROS reporters (e.g., hydroethidine) is $\Delta\psi_m$-dependent. This can affect their relative mitochondrial fluorescence signal (46, 135), and thereby confound assessment of the relationship between mitochondrial ROS production and $\Delta\psi_m$. During physiological conditions (FET), with mitochondria respiring on NADH-linked substrates, 30%–70% of mitochondrial ROS production is $\Delta\psi_m$-dependent. For instance, guinea pig isolated brain mitochondria respiring on NADH-linked substrates displayed a 30% decrease in $H_2O_2$ production upon complete $\Delta\psi_m$ dissipation (128). This suggests that ~60%–70% of this production was independent of $\Delta\psi_m$. In contrast, full $\Delta\psi_m$ dissipation reduced ROS production more significantly by ~70% in isolated rat brain mitochondria (126, 136). These results illustrate that the dependence of mitochondrial ROS production on $\Delta\psi_m$ depends on the experimental model and/or conditions. Taken together, it appears that a (variable) fraction of mitochondrial ROS production is $\Delta\psi_m$-independent and that there exists a "$\Delta\psi_m$ threshold," above which mitochondrial ROS production rapidly increases upon relatively small decreases (hyperpolarization) of $\Delta\psi_m$ (126). Such threshold behavior is likely to only occur when $\Delta\psi_m$ is hyperpolarized (i.e., more negative than −160 mV), which is likely to be lower than achievable in typical experimental systems (126, 136).

CIII-mediated ROS production is also $\Delta\psi_m$-dependent, in that it increases with increasing $\Delta\psi_m$ hyperpolarization. However, CIII-mediated ROS production likely becomes $\Delta\psi_m$-independent at more depolarized potentials (i.e., less negative than −150 mV) (15, 69).

To quantitatively explore the relationship between $\Delta\psi_m$ and mitochondrial ROS production, $\Delta\psi_m$ can be pharmacologically modulated by mitochondrial uncoupling (i.e., when ETC-mediated electron transport is not used to drive mitochondrial ATP synthesis). Uncoupling is achieved via induction of a trans-MIM proton influx or "leak". In cells, there is a basal unregulated trans-MIM proton leak (mainly determined by the fatty acyl composition of the membrane), and an inducible proton leak, mediated by mitochondrial uncoupling proteins (UCPs) (137, 138). Uncoupling can be pharmacologically induced by protonophores [e.g., carbonyl cyanide-*p*-trifluoromethoxyphenylhydrazone (FCCP) or carbonyl cyanide *m*-chlorophenyl hydrazone (CCCP)]. Such uncoupling induces $\Delta\psi_m$ depolarization and lowers mitochondrial ROS production (105, 126). For instance, FCCP treatment decreases both basal and rotenone-stimulated mitochondrial ROS production during FET (139). A similar role in reducing mitochondrial ROS production was suggested for UCPs (i.e., UCP2, UCP3) (140). Although one study suggested that basal FET-mediated mitochondrial ROS production was not affected by uncoupling nor by $\Delta\psi_m$ depolarization (141), the study acknowledged that $\Delta\psi_m$ may have depolarized below the ROS-affecting threshold. Given the existence of a $\Delta\psi_m$-dependence threshold for mitochondrial ROS generation, functions that allow simulation of different kinetics above and below this threshold (e.g., Hill or Boltzmann functions; Table 2), are suited to represent the biological system (121, 142).

CI-mediated ROS production is also $\Delta\psi_m$-dependent during RET (105, 126). This is compatible with the fact that a

highly negative $\Delta\psi_m$ is required to sustain RET, and that relatively small depolarizations (induced by promoting ATP synthesis or by mild uncoupling), significantly reduce RET-mediated ROS production (91, 105, 143, 144). Furthermore, it appears that RET-mediated mitochondrial ROS production increases with increasing ΔpH (145).

### $O_2$ Level and Consumption

Molecular oxygen ($O_2$) is the terminal electron acceptor in the ETC, being reduced to $H_2O$ by CIV. The rate of ETC-mediated ROS production positively correlates with the rate of mitochondrial $O_2$ consumption (146), with the fraction of $O_2$ converted into ROS being relatively low (i.e., between 0.1% and 4%) (147). Phenomenological models of mitochondrial ROS production have been developed based on the $O_2$ consumption rate (OCR) alone, and one such model calculated ROS production as a percentage of the simulated OCR (between 0.2% and 2%) (77). However, using OCR as a proxy of ETC-mediated ROS production has certain drawbacks. For instance, such models cannot discriminate between different sites of ROS production, and may not correctly predict ROS production during ETC inhibition. This is exemplified by the fact that inhibition of CIII by antimycin A decreases OCR. Models correlating ROS production to OCR will therefore predict decreased ROS production upon antimycin A treatment, whereas antimycin A is known to increase ROS production (see ROS PRODUCTION BY COMPLEX III). Similarly, mild uncoupling stimulates OCR, but decreases ROS generation (139, 148).

Mitochondrial ROS production is also affected by $O_2$ concentration ($[O_2]$), displaying a positive linear correlation within the supraphysiological $O_2$ range (21%) generally applied during in vitro experiments (16). The slope of this line depends on mitochondrial respiratory state (*state 3/4*; isolated brain mitochondria) (149). The latter study also demonstrated that this dependency may become nonlinear in the presence of mitochondrial inhibitors (149). In contrast, analysis of isolated liver mitochondria demonstrated that irrespective of the site of electron entry (i.e., CI, CII, or β-oxidation), ROS production displays a hyperbolic dependence on $[O_2]$. However, this observation might be due to a carboxylesterase enzyme present in liver mitochondria, which catalyzes formation of the fluorescent ROS-detecting molecule resorufin (149, 150). Interestingly, under hypoxic conditions (~1%–3% $O_2$) mitochondrial ROS production was increased, potentially due to activation of hypoxia-driven signaling (16, 151). As a final remark, different ROS-producing sites ($I_F$, $Q_O$) display different affinities for $O_2$ ($K_m$ values). This underlines the importance of including $[O_2]$ as a variable in ROS-predicting models (152).

### ROS Scavenging

For each type of ROS, its concentration at any cellular position in time depends on its rate of production, diffusion properties, membrane permeability, reactivity with other biomolecules (potentially inducing signaling and/or damage), and scavenging. With respect to the latter, a multitude of pathways exist in both mitochondria and cytosol (e.g., Fig. 1). When generated in the mitochondrial matrix, $O_2^{\cdot-}$ (which is not membrane permeable) is converted into $H_2O_2$ by SOD2/MnSOD. When generated in the IMS, this conversion is carried out by SOD1/CuSOD. Given that the concentration of SOD2 is in the μM range, matrix $O_2^{\cdot-}$ is converted to $H_2O_2$ at a relatively high rate (15, 45). $H_2O_2$ itself (which is membrane permeable) is converted into $H_2O$, both within the mitochondria and the cytosol, by the action of various enzymes (e.g., TRx, GPx, PRx, and catalase) or by reaction with nonenzymatic antioxidants (e.g., vitamin C, vitamin E, and GSH). Evidence in isolated brain mitochondria suggests that $H_2O_2$ scavenging is also a rapid process (15, 20). Several detailed mathematical models of ROS scavenging, including individual enzymes, were presented (e.g., Table 1). Given the rapid conversion of $O_2^{\cdot-}$ to $H_2O_2$, phenomenological equations often simulate ROS scavenging/emission from the mitochondria as a first-order process based on degradation rates of $H_2O_2$ alone (9, 20). Interestingly, unimpaired mitochondria appear to possess sufficient scavenging capacity to remove the majority of ROS generated during FET (15, 20). This suggests that impaired ROS scavenging is an important contributor to oxidative stress induction, rather than increased ROS production alone (15, 20).

## APPLYING PHENOMENOLOGICAL MODELS TO EXPLORE ROS-LINKED (PATHO) MECHANISMS

Phenomenological modeling of ETC-mediated ROS production has been applied for analysis of various ROS-associated (patho)physiologies. The most basic models assume a constant ROS production rate and have been applied to study downstream ROS effects. For example, modeling of lipid peroxidation provided evidence that the highly reactive ·OH radical is a primary initiator of this process, and demonstrated that vitamin E can efficiently block lipid peroxidation, in agreement with experimental studies (153). Another model suggested that $O_2^{\cdot-}$ is the most important ROS for molecular damage during aging (154). Phenomenological models have also been used to gain insight into the mechanistic aspects of ROS production. Focusing on the role of UCPs and mitochondrial ROS production in β-cells, analysis of a minimal model (including NADH, FADH, and $\Delta\psi_m$) highlighted that short-term UCP inhibition enhances ROS signaling, whereas long-term inhibition induces oxidative stress (121). The same group later developed a model of mitochondrial ROS production dependent on $QH_2$, and $\Delta\psi_m$ in which $[O_2]$ was constant (155). This suggested that the $QH_2$ level is a major regulator of mitochondrial ROS production. Another phenomenological model of OCR-dependent ROS production predicted that increased cytosolic free calcium ($Ca^{2+}$) levels induce increased levels of mitochondrial and cytosolic ROS (77, 156). Similarly, this model was used to illustrate the effects of pathological mitochondrial ROS levels on $Ca^{2+}$ homeostasis and cardiac excitability (157). Also linked to pathology, a model of ROS production dependent on $[O_2]$ and fatty acid oxidation was applied to elucidate the mechanisms underlying increased ischemia-reperfusion injury in fatty liver disease (158). Moreover, agent-based models [consisting of individual agents (e.g., mitochondria) and the interactions between them] have been used to investigate ROS-induced ROS release (142) and to study the effect of mitochondrial

network dynamics like density, size, distance between mitochondria, etc., on intermitochondrial ROS signaling (122).

To further demonstrate how phenomenological models may be applied to gain insight into disease pathology, we utilized a model recently developed in our group (159). This model integrates phenomenological equations of ETC-mediated ROS metabolism, as described earlier, with an ordinary differential equation (ODE)-based computational model of the ETC (160, 161). By simulating altered scavenging rates and ETC complex activity, it was predicted that impaired scavenging may have a greater impact on ETC-mediated ROS levels than ETC complex inhibition (159). This is compatible with previous studies suggesting that cells can generally cope with increased ROS levels mediated by pathological complex impairment, as long as scavenging mechanisms remain intact (5, 15, 20).

### Conclusions

ROS constitute reactive and damaging and/or signaling molecules that have been widely studied in (patho)physiology. Although aberrations in mitochondrial ROS generation have been observed in various pathologies, the exact mechanisms involved are still incompletely understood (21). Further improvement of experimental ROS analysis strategies is essential (22, 94). Although computational models have been successfully applied to analyze the intricacies of ROS metabolism beyond experimental investigation, the development of a complete mechanistic model of ETC-mediated ROS metabolism would be of great benefit (119). Detailed kinetic models, however, are by necessity inherently complex. A time-tested approach to overcome system complexity is to utilize phenomenological equations, and several such models have been applied to simulate various aspects of cellular ROS metabolism. Here we summarized ETC-mediated ROS production and scavenging mechanisms, detailed the primary ROS producing sites within the ETC during FET and RET, and highlighted their dependence on bioenergetic parameters like the $NADH/NAD^+$ ratio, the $QH_2/Q$ ratio, $\Delta\psi_m$, and $O_2$ concentration. We outlined how these empirical and/or theoretical dependencies can be harnessed to design phenomenological equations of ETC-mediated ROS metabolism and provided select examples of the application of such models to investigate ROS homeostasis. Accompanied by appropriate validation experiments, such models are useful to explore the mechanisms of ETC-mediated ROS metabolism and the role these mechanisms play in (patho)physiology.

## GRANTS

This project has received funding from the Innovative Medicines Initiative 2 Joint Undertaking under Grant Agreement No. 821522. This Joint Undertaking receives support from the European Union's Horizon 2020 Research and Innovation Program and European Federation of Pharmaceutical Industries and Associations (EFPIA) and Parkinson's UK. W. J. H. Koopman was supported by the Next Level Animal Sciences (NLAS) initiative ("Data and Models") of the Wageningen University (Wageningen, The Netherlands) and Radboudumc Principal Investigator (PI) support funding (Nijmegen, The Netherlands). This publication has emanated from research supported in part by a research grant from Science Foundation Ireland (SFI) under Grant No. 16/RC/3948 and cofunded under the European Regional Development Fund and by FutureNeuro industry partners.

## DISCLAIMERS

The material presented and views expressed here reflect the author's view and neither Innovative Medicines Initiative (IMI) nor the European Union, EFPIA, or any associated partners are responsible for any use that may be made of the information contained herein.

## DISCLOSURES

W. J. H. Koopman is an ad hoc scientific advisor of Khondrion B.V. (Nijmegen, The Netherlands). This company was not involved the writing of the manuscript, nor in the decision to submit the manuscript for publication. The other authors declare no conflict of interest.

## AUTHOR CONTRIBUTIONS

S.C. and N.M.C.C. interpreted results of experiments; S.C. and N.M.C.C. prepared figures; S.C., W.J.H.K., J.H.M.P., and N.M.C.C. drafted manuscript; S.C., W.J.H.K., J.H.M.P., and N.M.C.C. edited and revised manuscript; S.C., W.J.H.K., J.H.M.P., and N.M.C.C. approved final version of manuscript.

## REFERENCES

1. **Bell EL**, **Chandel NS.** Mitochondrial oxygen sensing: regulation of hypoxia-inducible factor by mitochondrial generated reactive oxygen species. *Essays Biochem* 43: 17–27, 2007. doi:10.1042/BSE0430017.
2. **Hinchy EC**, **Gruszczyk AV**, **Willows R**, **Navaratnam N**, **Hall AR**, **Bates G**, **Bright TP**, **Krieg T**, **Carling D**, **Murphy MP.** Mitochondria-derived ROS activate AMP-activated protein kinase (AMPK) indirectly. *J Biol Chem* 293: 17208–17217, 2018. doi:10.1074/jbc.RA118.002579.
3. **Sies H**, **Jones DP.** Reactive oxygen species (ROS) as pleiotropic physiological signalling agents. *Nat Rev Mol Cell Biol* 21: 363–383, 2020. doi:10.1038/s41580-020-0230-3.
4. **Sies H**, **Cadenas E.** Oxidative stress: damage to intact cells and organs. *Philos Trans R Soc Lond B Biol Sci* 311: 617–631, 1985. doi:10.1098/rstb.1985.0168.
5. **Andersen JK.** Oxidative stress in neurodegeneration: cause or consequence? *Nat Med* 10: S18–S25, 2004. doi:10.1038/nrn1434.
6. **Lin MT**, **Beal MF.** Mitochondrial dysfunction and oxidative stress in neurodegenerative diseases. *Nature* 443: 787–795, 2006. doi:10.1038/nature05292.
7. **Halliwell B.** Antioxidants in human health and disease. *Annu Rev Nutr* 16: 33–50, 1996. doi:10.1146/annurev.nu.16.070196.000341.
8. **Brand MD.** Mitochondrial generation of superoxide and hydrogen peroxide as the source of mitochondrial redox signaling. *Free Radic Biol Med* 100: 14–31, 2016. doi:10.1016/j.freeradbiomed.2016.04.001.
9. **Munro D**, **Treberg JR.** A radical shift in perspective: mitochondria as regulators of reactive oxygen species. *J Exp Biol* 220: 1170–1180, 2017. doi:10.1242/jeb.132142.
10. **Sena LA**, **Chandel NS.** Physiological roles of mitochondrial reactive oxygen species. *Mol Cell* 48: 158–167, 2012. doi:10.1016/j.molcel.2012.09.025.
11. **Han D**, **Antunes F**, **Canali R**, **Rettori D**, **Cadenas E.** Voltage-dependent anion channels control the release of the superoxide anion from mitochondria to cytosol. *J Biol Chem* 278: 5557–5563, 2003. doi:10.1074/jbc.M210269200.
12. **Sieprath T**, **Corne TD**, **Willems PH**, **Koopman WJ**, **De Vos WH.** Integrated high-content quantification of intracellular ROS levels and mitochondrial morphofunction. *Adv Anat Embryol Cell Biol* 219: 149–177, 2016. doi:10.1007/978-3-319-28549-8_6.
13. **Zhang Y**, **Wong HS.** Are mitochondria the main contributor of reactive oxygen species in cells? *J Exp Biol* 224: jeb221606, 2021. doi:10.1242/jeb.221606.
14. **Brown GC**, **Borutaite V.** There is no evidence that mitochondria are the main source of reactive oxygen species in mammalian cells. *Mitochondrion* 12: 1–4, 2012. doi:10.1016/j.mito.2011.02.001.

15. **Andreyev AY**, **Kushnareva YE**, **Starkov AA.** Mitochondrial metabolism of reactive oxygen species. *Biochemistry (Mosc)* 70: 200–214, 2005. doi:10.1007/s10541-005-0102-7.
16. **Murphy MP.** How mitochondria produce reactive oxygen species. *Biochem J* 417: 1–13, 2009. doi:10.1042/BJ20081386.
17. **Poljsak B.** Strategies for reducing or preventing the generation of oxidative stress. *Oxid Med Cell Longev* 2011: 194586, 2011. doi:10.1155/2011/194586.
18. **Chouchani ET**, **Pell VR**, **Gaude E**, **Aksentijevic D**, **Sundier SY**, **Robb EL**, **Logan A**, **Nadtochiy SM**, **Ord ENJ**, **Smith AC**, **Eyassu F**, **Shirley R**, **Hu CH**, **Dare AJ**, **James AM**, **Rogatti S**, **Hartley RC**, **Eaton S**, **Costa ASH**, **Brookes PS**, **Davidson SM**, **Duchen MR**, **Saeb-Parsy K**, **Shattock MJ**, **Robinson AJ**, **Work LM**, **Frezza C**, **Krieg T**, **Murphy MP.** Ischaemic accumulation of succinate controls reperfusion injury through mitochondrial ROS. *Nature* 515: 431–435, 2014. doi:10.1038/nature13909.
19. **Wong HS**, **Dighe PA**, **Mezera V**, **Monternier PA**, **Brand MD.** Production of superoxide and hydrogen peroxide from specific mitochondrial sites under different bioenergetic conditions. *J Biol Chem* 292: 16804–16809, 2017. doi:10.1074/jbc.R117.789271.
20. **Starkov AA**, **Andreyev AY**, **Zhang SF**, **Starkova NN**, **Korneeva M**, **Syromyatnikov M**, **Popov VN.** Scavenging of $H_2O_2$ by mouse brain mitochondria. *J Bioenerg Biomembr* 46: 471–477, 2014. doi:10.1007/s10863-014-9581-9.
21. **Andreyev AY**, **Kushnareva YE**, **Murphy AN**, **Starkov AA.** Mitochondrial ROS metabolism: 10 years later. *Biochemistry (Mosc)* 80: 517–531, 2015. doi:10.1134/S0006297915050028.
22. **Pak VV**, **Ezerina D**, **Lyublinskaya OG**, **Pedre B**, **Tyurin-Kuzmin PA**, **Mishina NM**, **Thauvin M**, **Young D**, **Wahni K**, **Martínez Gache SA**, **Demidovich AD**, **Ermakova YG**, **Maslova YD**, **Shokhina AG**, **Eroglu E**, **Bilan DS**, **Bogeski I**, **Michel T**, **Vriz S**, **Messens J**, **Belousov VV.** Ultrasensitive genetically encoded indicator for hydrogen peroxide identifies roles for the oxidant in cell migration and mitochondrial function. *Cell Metab* 31: 642–653.e6, 2020. doi:10.1016/j.cmet.2020.02.003.
23. **Kiley PJ**, **Storz G.** Exploiting thiol modifications. *PLoS Biol* 2: e400, 2004. doi:10.1371/journal.pbio.0020400.
24. **Sies H**, **Berndt C**, **Jones DP.** Oxidative stress. *Annu Rev Biochem* 86: 715–748, 2017. doi:10.1146/annurev-biochem-061516-045037.
25. **Wang Y**, **Branicky R**, **Noe A**, **Hekimi S.** Superoxide dismutases: dual roles in controlling ROS damage and regulating ROS signaling. *J Cell Biol* 217: 1915–1928, 2018. doi:10.1083/jcb.201708007.
26. **Winterbourn CC.** Toxicity of iron and hydrogen peroxide: the Fenton reaction. *Toxicol Lett*82–83: 969–974, 1995. doi:10.1016/0378-4274(95)03532-x.
27. **Bindokas VP**, **Jordan J**, **Lee CC**, **Miller RJ.** Superoxide production in rat hippocampal neurons: selective imaging with hydroethidine. *J Neurosci* 16: 1324–1336, 1996. doi:10.1523/JNEUROSCI.16-04-01324.1996.
28. **Halliwell B**, **Whiteman M.** Measuring reactive species and oxidative damage in vivo and in cell culture: how should you do it and what do the results mean? *Br J Pharmacol* 142: 231–255, 2004. doi:10.1038/sj.bjp.0705776.
29. **Giustarini D**, **Dalle-Donne I**, **Tsikas D**, **Rossi R.** Oxidative stress and human diseases: origin, link, measurement, mechanisms, and biomarkers. *Crit Rev Clin Lab Sci* 46: 241–281, 2009. doi:10.3109/10408360903142326.
30. **Forkink M**, **Smeitink JA**, **Brock R**, **Willems PH**, **Koopman WJ.** Detection and manipulation of mitochondrial reactive oxygen species in mammalian cells. *Biochim Biophys Acta* 1797: 1034–1044, 2010. doi:10.1016/j.bbabio.2010.01.022.
31. **Dikalov SI**, **Harrison DG.** Methods for detection of mitochondrial and cellular reactive oxygen species. *Antioxid Redox Signal* 20: 372–382, 2014. doi:10.1089/ars.2012.4886.
32. **Oparka M**, **Walczak J**, **Malinska D**, **van Oppen L**, **Szczepanowska J**, **Koopman WJH**, **Wieckowski MR.** Quantifying ROS levels using CM-H2DCFDA and HyPer. *Methods* 109: 3–11, 2016. doi:10.1016/j.ymeth.2016.06.008.
33. **Gao P**, **Pan W**, **Li N**, **Tang B.** Fluorescent probes for organelle-targeted bioactive species imaging. *Chem Sci* 10: 6035–6071, 2019. doi:10.1039/c9sc01652j.
34. **Mailloux RJ.** An update on methods and approaches for interrogating mitochondrial reactive oxygen species production. *Redox Biol* 45: 102044, 2021. doi:10.1016/j.redox.2021.102044.
35. **Belousov VV**, **Fradkov AF**, **Lukyanov KA**, **Staroverov DB**, **Shakhbazov KS**, **Terskikh AV**, **Lukyanov S.** Genetically encoded fluorescent indicator for intracellular hydrogen peroxide. *Nat Methods* 3: 281–286, 2006. doi:10.1038/nmeth866.
36. **Koopman WJ**, **Verkaart S**, **van Emst-de Vries SE**, **Grefte S**, **Smeitink JA**, **Willems PH.** Simultaneous quantification of oxidative stress and cell spreading using 5-(and-6)-chloromethyl-2',7'-dichlorofluorescein. *Cytometry A* 69: 1184–1192, 2006. doi:10.1002/cyto.a.20348.
37. **Dickinson BC**, **Srikun D**, **Chang CJ.** Mitochondrial-targeted fluorescent probes for reactive oxygen species. *Curr Opin Chem Biol* 14: 50–56, 2010. doi:10.1016/j.cbpa.2009.10.014.
38. **Polster BM**, **Nicholls DG**, **Ge SX**, **Roelofs BA.** Use of potentiometric fluorophores in the measurement of mitochondrial reactive oxygen species. *Methods Enzymol* 547: 225–250, 2014. doi:10.1016/B978-0-12-801415-8.00013-8.
39. **Grefte S**, **Koopman WJH.** Live-cell assessment of reactive oxygen species levels using dihydroethidine. *Methods Mol Biol* 2275: 291–299, 2021. doi:10.1007/978-1-0716-1262-0_18.
40. **Boveris A**, **Valdez LB**, **Zaobornyj T**, **Bustamante J.** Mitochondrial metabolic states regulate nitric oxide and hydrogen peroxide diffusion to the cytosol. *Biochim Biophys Acta* 1757: 535–542, 2006. doi:10.1016/j.bbabio.2006.02.010.
41. **Ferrer-Sueta G**, **Radi R.** Chemical biology of peroxynitrite: kinetics, diffusion, and radicals. *ACS Chem Biol* 4: 161–177, 2009. doi:10.1021/cb800279q.
42. **Koopman WJ**, **Nijtmans LG**, **Dieteren CE**, **Roestenberg P**, **Valsecchi F**, **Smeitink JA**, **Willems PH.** Mammalian mitochondrial complex I: biogenesis, regulation, and reactive oxygen species generation. *Antioxid Redox Signal* 12: 1431–1470, 2010 [Erratum in *Antioxid Redox Signal* 36: 187–188, 2022]. doi:10.1089/ars.2009.2743.
43. **Forkink M**, **Basit F**, **Teixeira J**, **Swarts HG**, **Koopman WJH**, **Willems P.** Complex I and complex III inhibition specifically increase cytosolic hydrogen peroxide levels without inducing oxidative stress in HEK293 cells. *Redox Biol* 6: 607–616, 2015. doi:10.1016/j.redox.2015.09.003.
44. **Millare B**, **O'Rourke B**, **Trayanova N.** Hydrogen peroxide diffusion and scavenging shapes mitochondrial network instability and failure by sensitizing ROS-induced ROS release. *Sci Rep* 10: 15758, 2020. doi:10.1038/s41598-020-71308-z.
45. **Murphy MP**, **Holmgren A**, **Larsson NG**, **Halliwell B**, **Chang CJ**, **Kalyanaraman B**, **Rhee SG**, **Thornalley PJ**, **Partridge L**, **Gems D**, **Nystrom T**, **Belousov V**, **Schumacker PT**, **Winterbourn CC.** Unraveling the biological roles of reactive oxygen species. *Cell Metab* 13: 361–366, 2011. doi:10.1016/j.cmet.2011.03.010.
46. **Connolly NMC**, **Theurey P**, **Adam-Vizi V**, **Bazan NG**, **Bernardi P**, **Bolanos JP** et al. Guidelines on experimental methods to assess mitochondrial dysfunction in cellular models of neurodegenerative diseases. *Cell Death Differ* 25: 542–572, 2018. doi:10.1038/s41418-017-0020-4.
47. **Hoehne MN**, **Jacobs L**, **Lapacz KJ**, **Calabrese G**, **Murschall LM**, **Marker T**, **Kaul H**, **Trifunovic A**, **Morgan B**, **Fricker M**, **Belousov VV**, **Riemer J.** Spatial and temporal control of mitochondrial H2 O2 release in intact human cells. *EMBO J* 41: e109169, 2022. doi:10.15252/embj.2021109169.
48. **Wojtovich AP**, **Foster TH.** Optogenetic control of ROS production. *Redox Biol* 2: 368–376, 2014. doi:10.1016/j.redox.2014.01.019.
49. **Paardekooper LM**, **van Vroonhoven E**, **Ter Beest M**, **van den Bogaart G.** Radical stress is more cytotoxic in the nucleus than in other organelles. *Int J Mol Sci* 20: 4147, 2019. doi:10.3390/ijms20174147.
50. **Hodgkin AL**, **Huxley AF.** A quantitative description of membrane current and its application to conduction and excitation in nerve. *J Physiol* 117: 500–544, 1952. doi:10.1113/jphysiol.1952.sp004764.
51. **Goldbeter A**, **Dupont G**, **Berridge MJ.** Minimal model for signal-induced $Ca^{2+}$ oscillations and for their frequency encoding through protein phosphorylation. *Proc Natl Acad Sci USA* 87: 1461–1465, 1990. doi:10.1073/pnas.87.4.1461.
52. **Tyson JJ**, **Chen KC**, **Novak B.** Sniffers, buzzers, toggles and blinkers: dynamics of regulatory and signaling pathways in the cell. *Curr Opin Cell Biol* 15: 221–231, 2003. doi:10.1016/s0955-0674(03)00017-6.
53. **Dieteren CE**, **Gielen SC**, **Nijtmans LG**, **Smeitink JA**, **Swarts HG**, **Brock R**, **Willems PH**, **Koopman WJ.** Solute diffusion is hindered in the mitochondrial matrix. *Proc Natl Acad Sci USA* 108: 8657–8662, 2011. doi:10.1073/pnas.1017581108.

54. **Alam MT**, **Manjeri GR**, **Rodenburg RJ**, **Smeitink JA**, **Notebaart RA**, **Huynen M**, **Willems PH**, **Koopman WJ.** Skeletal muscle mitochondria of NDUFS4$^{-/-}$ mice display normal maximal pyruvate oxidation and ATP production. *Biochim Biophys Acta* 1847: 526–533, 2015. doi:10.1016/j.bbabio.2015.02.006.
55. **Liemburg-Apers DC**, **Schirris TJ**, **Russel FG**, **Willems PH**, **Koopman WJ.** Mitoenergetic dysfunction triggers a rapid compensatory increase in steady-state glucose flux. *Biophys J* 109: 1372–1386, 2015. doi:10.1016/j.bpj.2015.08.002.
56. **Markram H**, **Muller E**, **Ramaswamy S**, **Reimann MW**, **Abdellah M**, **Sanchez CA** et al. Reconstruction and simulation of neocortical microcircuitry. *Cell* 163: 456–492, 2015. doi:10.1016/j.cell.2015.09.029.
57. **Nielsen J.** Systems biology of metabolism. *Annu Rev Biochem* 86: 245–275, 2017. doi:10.1146/annurev-biochem-061516-044757.
58. **Niebel B**, **Leupold S**, **Heinemann M.** An upper limit on Gibbs energy dissipation governs cellular metabolism. *Nat Metab* 1: 125–132, 2019. doi:10.1038/s42255-018-0006-7.
59. **Schleicher J.** Introduction to in silico modeling to study ROS dynamics. *Methods Mol Biol* 2202: 1–32, 2021. doi:10.1007/978-1-0716-0896-8_1.
60. **Bazil JN**, **Pannala VR**, **Dash RK**, **Beard DA.** Determining the origins of superoxide and hydrogen peroxide in the mammalian NADH: ubiquinone oxidoreductase. *Free Radic Biol Med* 77: 121–129, 2014. doi:10.1016/j.freeradbiomed.2014.08.023.
61. **Manhas N**, **Duong QV**, **Lee P**, **Richardson JD**, **Robertson JD**, **Moxley MA**, **Bazil JN.** Computationally modeling mammalian succinate dehydrogenase kinetics identifies the origins and primary determinants of ROS production. *J Biol Chem* 295: 15262–15279, 2020. doi:10.1074/jbc.RA120.014483.
62. **Markevich NI**, **Galimova MH**, **Markevich LN.** Hysteresis and bistability in the succinate-CoQ reductase activity and reactive oxygen species production in the mitochondrial respiratory complex II. *Redox Biol* 37: 101630, 2020. doi:10.1016/j.redox.2020.101630.
63. **Selivanov VA**, **Votyakova TV**, **Zeak JA**, **Trucco M**, **Roca J**, **Cascante M.** Bistability of mitochondrial respiration underlies paradoxical reactive oxygen species generation induced by anoxia. *PLoS Comput Biol* 5: e1000619, 2009. doi:10.1371/journal.pcbi.1000619.
64. **Quinlan CL**, **Gerencser AA**, **Treberg JR**, **Brand MD.** The mechanism of superoxide production by the antimycin-inhibited mitochondrial Q-cycle. *J Biol Chem* 286: 31361–31372, 2011. doi:10.1074/jbc.M111.267898.
65. **Bazil JN**, **Vinnakota KC**, **Wu F**, **Beard DA.** Analysis of the kinetics and bistability of ubiquinol: cytochrome c oxidoreductase. *Biophys J* 105: 343–355, 2013. doi:10.1016/j.bpj.2013.05.033.
66. **Guillaud F**, **Drose S**, **Kowald A**, **Brandt U**, **Klipp E.** Superoxide production by cytochrome bc1 complex: a mathematical model. *Biochim Biophys Acta* 1837: 1643–1652, 2014. doi:10.1016/j.bbabio.2014.05.358.
67. **Selivanov VA**, **Votyakova TV**, **Pivtoraiko VN**, **Zeak J**, **Sukhomlin T**, **Trucco M**, **Roca J**, **Cascante M.** Reactive oxygen species production by forward and reverse electron fluxes in the mitochondrial respiratory chain. *PLoS Comput Biol* 7: e1001115, 2011. doi:10.1371/journal.pcbi.1001115.
68. **Selivanov VA**, **Cascante M**, **Friedman M**, **Schumaker MF**, **Trucco M**, **Votyakova TV.** Multistationary and oscillatory modes of free radicals generation by the mitochondrial respiratory chain revealed by a bifurcation analysis. *PLoS Comput Biol* 8: e1002700, 2012. doi:10.1371/journal.pcbi.1002700.
69. **Gauthier LD**, **Greenstein JL**, **Cortassa S**, **O'Rourke B**, **Winslow RL.** A computational model of reactive oxygen species and redox balance in cardiac mitochondria. *Biophys J* 105: 1045–1056, 2013. doi:10.1016/j.bpj.2013.07.006.
70. **Magnus G**, **Keizer J.** Model of β-cell mitochondrial calcium handling and electrical activity. I. Cytoplasmic variables. *Am J Physiol Cell Physiol* 274: C1158–C1173, 1998. doi:10.1152/ajpcell.1998.274.4.C1158.
71. **Demin OV**, **Kholodenko BN**, **Skulachev VP.** A model of $O_2.^-$ generation in the complex III of the electron transport chain. *Mol Cell Biochem* 184: 21–33, 1998.
72. **Demin OV**, **Gorianin II**, **Kholodenko BN**, **Westerhoff HV.** [Kinetic modeling of energy metabolism and generation of active forms of oxygen in hepatocyte mitochondria]. *Mol Biol (Mosk)* 35: 1095–1104, 2001.
73. **Markevich NI**, **Hoek JB.** Computational modeling analysis of mitochondrial superoxide production under varying substrate conditions and upon inhibition of different segments of the electron transport chain. *Biochim Biophys Acta* 1847: 656–679, 2015. doi:10.1016/j.bbabio.2015.04.005.
74. **Duong QV**, **Levitsky Y**, **Dessinger MJ**, **Strubbe-Rivera JO**, **Bazil JN.** Identifying site-specific superoxide and hydrogen peroxide production rates from the mitochondrial electron transport system using a computational strategy. *Function (Oxf)* 2: zqab050, 2021. doi:10.1093/function/zqab050.
75. **Bazil JN**, **Beard DA**, **Vinnakota KC.** Catalytic coupling of oxidative phosphorylation, ATP demand, and reactive oxygen species generation. *Biophys J* 110: 962–971, 2016. doi:10.1016/j.bpj.2015.09.036.
76. **Kembro JM**, **Aon MA**, **Winslow RL**, **O'Rourke B**, **Cortassa S.** Integrating mitochondrial energetics, redox and ROS metabolic networks: a two-compartment model. *Biophys J* 104: 332–343, 2013. doi:10.1016/j.bpj.2012.11.3808.
77. **Cortassa S**, **Aon MA**, **Winslow RL**, **O'Rourke B.** A mitochondrial oscillator dependent on reactive oxygen species. *Biophys J* 87: 2060–2073, 2004. doi:10.1529/biophysj.104.041749.
78. **Aon MA**, **Stanley BA**, **Sivakumaran V**, **Kembro JM**, **O'Rourke B**, **Paolocci N**, **Cortassa S.** Glutathione/thioredoxin systems modulate mitochondrial $H_2O_2$ emission: an experimental-computational study. *J Gen Physiol* 139: 479–491, 2012. doi:10.1085/jgp.201210772.
79. **Kembro JM**, **Cortassa S**, **Lloyd D**, **Sollott SJ**, **Aon MA.** Mitochondrial chaotic dynamics: Redox-energetic behavior at the edge of stability. *Sci Rep* 8: 15422, 2018. doi:10.1038/s41598-018-33582-w.
80. **Zhou L**, **Aon MA**, **Almas T**, **Cortassa S**, **Winslow RL**, **O'Rourke B.** A reaction-diffusion model of ROS-induced ROS release in a mitochondrial network. *PLoS Comput Biol* 6: e1000657, 2010. doi:10.1371/journal.pcbi.1000657.
81. **Pannala VR**, **Bazil JN**, **Camara AK**, **Dash RK.** A biophysically based mathematical model for the catalytic mechanism of glutathione reductase. *Free Radic Biol Med* 65: 1385–1397, 2013. doi:10.1016/j.freeradbiomed.2013.10.001.
82. **Gizzatkulov NM**, **Goryanin II**, **Metelkin EA**, **Mogilevskaya EA**, **Peskov KV**, **Demin OV.** DBSolve Optimum: a software package for kinetic modeling which allows dynamic visualization of simulation results. *BMC Syst Biol* 4: 109, 2010. doi:10.1186/1752-0509-4-109.
83. **Bruggeman FJ**, **Westerhoff HV.** Approaches to biosimulation of cellular processes. *J Biol Phys* 32: 273–288, 2006. doi:10.1007/s10867-006-9016-x.
84. **Ransac S**, **Parisey N**, **Mazat JP.** The loneliness of the electrons in the bc1 complex. *Biochim Biophys Acta* 1777: 1053–1059, 2008. doi:10.1016/j.bbabio.2008.05.003.
85. **Ransac S**, **Arnarez C**, **Mazat JP.** The flitting of electrons in complex I: a stochastic approach. *Biochim Biophys Acta* 1797: 641–648, 2010. doi:10.1016/j.bbabio.2010.03.011.
86. **Hock DH**, **Robinson DRL**, **Stroud DA.** Blackout in the powerhouse: clinical phenotypes associated with defects in the assembly of OXPHOS complexes and the mitoribosome. *Biochem J* 477: 4085–4132, 2020. doi:10.1042/BCJ20190767.
87. **Letts JA**, **Sazanov LA.** Clarifying the supercomplex: the higher-order organization of the mitochondrial electron transport chain. *Nat Struct Mol Biol* 24: 800–808, 2017. doi:10.1038/nsmb.3460.
88. **Koopman WJ**, **Distelmaier F**, **Esseling JJ**, **Smeitink JA**, **Willems PH.** Computer-assisted live cell analysis of mitochondrial membrane potential, morphology and calcium handling. *Methods* 46: 304–311, 2008. doi:10.1016/j.ymeth.2008.09.018.
89. **Nicholls DG.** *Bioenergetics*. Cambridge, MA: Academic Press, 2013.
90. **Mailloux RJ.** Teaching the fundamentals of electron transfer reactions in mitochondria and the production and detection of reactive oxygen species. *Redox Biol* 4: 381–398, 2015. doi:10.1016/j.redox.2015.02.001.
91. **Adam-Vizi V**, **Chinopoulos C.** Bioenergetics and the formation of mitochondrial reactive oxygen species. *Trends Pharmacol Sci* 27: 639–645, 2006. doi:10.1016/j.tips.2006.10.005.
92. **Quinlan CL**, **Perevoshchikova IV**, **Hey-Mogensen M**, **Orr AL**, **Brand MD.** Sites of reactive oxygen species generation by mitochondria oxidizing different substrates. *Redox Biol* 1: 304–312, 2013. doi:10.1016/j.redox.2013.04.005.
93. **Quinlan CL**, **Orr AL**, **Perevoshchikova IV**, **Treberg JR**, **Ackrell BA**, **Brand MD.** Mitochondrial complex II can generate reactive oxygen

species at high rates in both the forward and reverse reactions. *J Biol Chem* 287: 27255–27264, 2012. doi:10.1074/jbc.M112.374629.
94. **Hernansanz-Agustin P**, **Enriquez JA.** Generation of reactive oxygen species by mitochondria. *Antioxidants (Basel)* 10: 1–13, 2021. doi:10.1042/BJ20081386.
95. **Kamarauskaite J**, **Baniene R**, **Trumbeckas D**, **Strazdauskas A**, **Trumbeckaite S.** Increased succinate accumulation induces ROS generation in in vivo ischemia/reperfusion-affected rat kidney mitochondria. *Biomed Res Int* 2020: 8855585, 2020. doi:10.1155/2020/8855585.
96. **Mills EL**, **Kelly B**, **Logan A**, **Costa ASH**, **Varma M**, **Bryant CE**, **Tourlomousis P**, **Dabritz JHM**, **Gottlieb E**, **Latorre I**, **Corr SC**, **McManus G**, **Ryan D**, **Jacobs HT**, **Szibor M**, **Xavier RJ**, **Braun T**, **Frezza C**, **Murphy MP**, **O'Neill LA.** Succinate dehydrogenase supports metabolic repurposing of mitochondria to drive inflammatory macrophages. *Cell* 167: 457–470, 2016. doi:10.1016/j.cell.2016.08.064.
97. **Raimondi V**, **Ciccarese F**, **Ciminale V.** Oncogenic pathways and the electron transport chain: a dangeROS liaison. *Br J Cancer* 122: 168–181, 2020. doi:10.1038/s41416-019-0651-y.
98. **Zhu J**, **Vinothkumar KR**, **Hirst J.** Structure of mammalian respiratory complex I. *Nature* 536: 354–358, 2016. doi:10.1038/nature19095.
99. **Sazanov LA**, **Hinchliffe P.** Structure of the hydrophilic domain of respiratory complex I from *Thermus thermophilus*. *Science* 311: 1430–1436, 2006. doi:10.1126/science.1123809.
100. **Brandt U.** Energy converting NADH:quinone oxidoreductase (complex I). *Annu Rev Biochem* 75: 69–92, 2006. doi:10.1146/annurev.biochem.75.103004.142539.
101. **Baradaran R**, **Berrisford JM**, **Minhas GS**, **Sazanov LA.** Crystal structure of the entire respiratory complex I. *Nature* 494: 443–448, 2013. doi:10.1038/nature11871.
102. **Cobley JN.** Mechanisms of mitochondrial ROS in assisted reproduction: the known, the unknown, and the intriguing. *Antioxidants* 9: 933, 2020. doi:10.3390/antiox9100933.
103. **Fendel U**, **Tocilescu MA**, **Kerscher S**, **Brandt U.** Exploring the inhibitor binding pocket of respiratory complex I. *Biochim Biophys Acta* 1777: 660–665, 2008. doi:10.1016/j.bbabio.2008.04.033.
104. **Lopez-Fabuel I**, **Le Douce J**, **Logan A**, **James AM**, **Bonvento G**, **Murphy MP**, **Almeida A**, **Bolanos JP.** Complex I assembly into supercomplexes determines differential mitochondrial ROS production in neurons and astrocytes. *Proc Natl Acad Sci USA* 113: 13063–13068, 2016. doi:10.1073/pnas.1613701113.
105. **Votyakova TV**, **Reynolds IJ.** $\gamma\psi_m$-dependent and -independent production of reactive oxygen species by rat brain mitochondria. *J Neurochem* 79: 266–277, 2001. doi:10.1046/j.1471-4159.2001.00548.x.
106. **Vinogradov AD**, **Grivennikova VG.** Oxidation of NADH and ROS production by respiratory complex I. *Biochim Biophys Acta* 1857: 863–871, 2016. doi:10.1016/j.bbabio.2015.11.004.
107. **Schonfeld P**, **Wojtczak L.** Fatty acids decrease mitochondrial generation of reactive oxygen species at the reverse electron transport but increase it at the forward transport. *Biochim Biophys Acta* 1767: 1032–1040, 2007. doi:10.1016/j.bbabio.2007.04.005.
108. **Robb EL**, **Hall AR**, **Prime TA**, **Eaton S**, **Szibor M**, **Viscomi C**, **James AM**, **Murphy MP.** Control of mitochondrial superoxide production by reverse electron transport at complex I. *J Biol Chem* 293: 9869–9879, 2018 [Erratum in *J Biol Chem* 294: 7966, 2019]. doi:10.1074/jbc.RA118.003647.
109. **Yin Z**, **Burger N**, **Kula-Alwar D**, **Aksentijevic D**, **Bridges HR**, **Prag HA**, **Grba DN**, **Viscomi C**, **James AM**, **Mottahedin A**, **Krieg T**, **Murphy MP**, **Hirst J.** Structural basis for a complex I mutation that blocks pathological ROS production. *Nat Commun* 12: 707, 2021. doi:10.1038/s41467-021-20942-w.
110. **Lambert AJ**, **Buckingham JA**, **Boysen HM**, **Brand MD.** Diphenyleneiodonium acutely inhibits reactive oxygen species production by mitochondrial complex I during reverse, but not forward electron transport. *Biochim Biophys Acta* 1777: 397–403, 2008. doi:10.1016/j.bbabio.2008.03.005.
111. **Scialò F**, **Fernández-Ayala DJ**, **Sanz A.** Role of mitochondrial reverse electron transport in ROS signaling: potential roles in health and disease. *Front Physiol* 8: 428, 2017. doi:10.3389/fphys.2017.00428.
112. **Onukwufor JO**, **Berry BJ**, **Wojtovich AP.** Physiologic implications of reactive oxygen species production by mitochondrial complex I reverse electron transport. *Antioxidants* 8: 285, 2019. doi:10.3390/antiox8080285.
113. **Quinlan CL**, **Treberg JR**, **Brand MD.** Mechanisms of mitochondrial free radical production and their relationship to the aging process. In: *Handbook of the Biology of Aging*, edited by Masoro EJ, Austad SN, Amsterdam, The Netherlands. doi:10.1016/B978-0-12-378638-8.00003-8, 2011, p. 47–61.
114. **Saraste M.** Oxidative phosphorylation at the fin de siecle. *Science* 283: 1488–1493, 1999. doi:10.1126/science.283.5407.1488.
115. **Bleier L**, **Drose S.** Superoxide generation by complex III: from mechanistic rationales to functional consequences. *Biochim Biophys Acta* 1827: 1320–1331, 2013. doi:10.1016/j.bbabio.2012.12.002.
116. **Kushnareva Y**, **Murphy AN**, **Andreyev A.** Complex I-mediated reactive oxygen species generation: modulation by cytochrome c and NAD(P)+ oxidation-reduction state. *Biochem J* 368: 545–553, 2002. doi:10.1042/BJ20021121.
117. **Zmijewski JW**, **Lorne E**, **Banerjee S**, **Abraham E.** Participation of mitochondrial respiratory complex III in neutrophil activation and lung injury. *Am J Physiol Lung Cell Mol Physiol* 296: L624–L634, 2009. doi:10.1152/ajplung.90522.2008.
118. **Pereira EJ**, **Smolko CM**, **Janes KA.** Computational models of reactive oxygen species as metabolic byproducts and signal-transduction modulators. *Front Pharmacol* 7: 457, 2016. doi:10.3389/fphar.2016.00457.
119. **Mazat JP**, **Devin A**, **Ransac S.** Modelling mitochondrial ROS production by the respiratory chain. *Cell Mol Life Sci* 77: 455–465, 2020. doi:10.1007/s00018-019-03381-1.
120. **Aldridge BB**, **Burke JM**, **Lauffenburger DA**, **Sorger PK.** Physicochemical modelling of cell signalling pathways. *Nat Cell Biol* 8: 1195–1203, 2006. doi:10.1038/ncb1497.
121. **Heuett WJ**, **Periwal V.** Autoregulation of free radicals via uncoupling protein control in pancreatic β-cell mitochondria. *Biophys J* 98: 207–217, 2010. doi:10.1016/j.bpj.2009.10.012.
122. **Park J**, **Lee J**, **Choi C.** Mitochondrial network determines intracellular ROS dynamics and sensitivity to oxidative stress through switching inter-mitochondrial messengers. *PLoS One* 6: e23211, 2011. doi:10.1371/journal.pone.0023211.
123. **Wilhelm F**, **Hirrlinger J.** Multifunctional roles of NAD+ and NADH in astrocytes. *Neurochem Res* 37: 2317–2325, 2012. doi:10.1007/s11064-012-0760-y.
124. **Kussmaul L**, **Hirst J.** The mechanism of superoxide production by NADH: ubiquinone oxidoreductase (complex I) from bovine heart mitochondria. *Proc Natl Acad Sci USA* 103: 7607–7612, 2006. doi:10.1073/pnas.0510977103.
125. **Korge P**, **Calmettes G**, **Weiss JN.** Reactive oxygen species production in cardiac mitochondria after complex I inhibition: modulation by substrate-dependent regulation of the NADH/$NAD^+$ ratio. *Free Radic Biol Med* 96: 22–33, 2016. doi:10.1016/j.freeradbiomed.2016.04.002.
126. **Starkov AA**, **Fiskum G.** Regulation of brain mitochondrial $H_2O_2$ production by membrane potential and NAD(P)H redox state. *J Neurochem* 86: 1101–1107, 2003. doi:10.1046/j.1471-4159.2003.01908.x.
127. **Kudin AP**, **Bimpong-Buta NY-B**, **Vielhaber S**, **Elger CE**, **Kunz WS.** Characterization of superoxide-producing sites in isolated brain mitochondria. *J Biol Chem* 279: 4127–4135, 2004. doi:10.1074/jbc.M310341200.
128. **Tretter L**, **Adam-Vizi V.** Moderate dependence of ROS formation on $\Delta\Psi_m$ in isolated brain mitochondria supported by NADH-linked substrates. *Neurochem Res* 32: 569–575, 2007. doi:10.1007/s11064-006-9130-y.
129. **Lambert AJ**, **Buckingham JA**, **Brand MD.** Dissociation of superoxide production by mitochondrial complex I from NAD(P)H redox state. *FEBS Lett* 582: 1711–1714, 2008. doi:10.1016/j.febslet.2008.04.030.
130. **Kareyeva AV**, **Grivennikova VG**, **Vinogradov AD.** Mitochondrial hydrogen peroxide production as determined by the pyridine nucleotide pool and its redox state. *Biochim Biophys Acta* 1817: 1879–1885, 2012. doi:10.1016/j.bbabio.2012.03.033.
131. **Watson MA**, **Wong HS**, **Brand MD.** Use of S1QELs and S3QELs to link mitochondrial sites of superoxide and hydrogen peroxide generation to physiological and pathological outcomes. *Biochem Soc Trans* 47: 1461–1469, 2019. doi:10.1042/BST20190305.

132. **Sarewicz M**, **Osyczka A.** Electronic connection between the quinone and cytochrome c redox pools and its role in regulation of mitochondrial electron transport and redox signaling. *Physiol Rev* 95: 219–243, 2015. doi:10.1152/physrev.00006.2014.
133. **Chinopoulos C.** The "B space" of mitochondrial phosphorylation. *J Neurosci Res* 89: 1897–1904, 2011. doi:10.1002/jnr.22659.
134. **Selivanov VA**, **Zeak JA**, **Roca J**, **Cascante M**, **Trucco M**, **Votyakova TV.** The role of external and matrix pH in mitochondrial reactive oxygen species generation. *J Biol Chem* 283: 29292–29300, 2008. doi:10.1074/jbc.M801019200.
135. **Koopman WJ**, **Verkaart S**, **Visch HJ**, **van der Westhuizen FH**, **Murphy MP**, **van den Heuvel LW**, **Smeitink JA**, **Willems PH.** Inhibition of complex I of the electron transport chain causes O2.$^-$-mediated mitochondrial outgrowth. *Am J Physiol Cell Physiol* 288: C1440–C1450, 2005. doi:10.1152/ajpcell.00607.2004.
136. **Starkov AA**, **Polster BM**, **Fiskum G.** Regulation of hydrogen peroxide production by brain mitochondria by calcium and Bax. *J Neurochem* 83: 220–228, 2002. doi:10.1046/j.1471-4159.2002.01153.x.
137. **Cannon B**, **Shabalina IG**, **Kramarova TV**, **Petrovic N**, **Nedergaard J.** Uncoupling proteins: a role in protection against reactive oxygen species–or not? *Biochim Biophys Acta* 1757: 449–458, 2006. doi:10.1016/j.bbabio.2006.05.016.
138. **Busiello RA**, **Savarese S**, **Lombardi A.** Mitochondrial uncoupling proteins and energy metabolism. *Front Physiol* 6: 36, 2015. doi:10.3389/fphys.2015.00036.
139. **Dlaskova A**, **Hlavata L**, **Jezek J**, **Jezek P.** Mitochondrial complex I superoxide production is attenuated by uncoupling. *Int J Biochem Cell Biol* 40: 2098–2109, 2008. doi:10.1016/j.biocel.2008.02.007.
140. **Mailloux RJ**, **Harper ME.** Uncoupling proteins and the control of mitochondrial reactive oxygen species production. *Free Radic Biol Med* 51: 1106–1115, 2011. doi:10.1016/j.freeradbiomed.2011.06.022.
141. **Tretter L**, **Adam-Vizi V.** Uncoupling is without an effect on the production of reactive oxygen species by in situ synaptic mitochondria. *J Neurochem* 103: 1864–1871, 2007. doi:10.1111/j.1471-4159.2007.04891.x.
142. **Nivala M**, **Korge P**, **Nivala M**, **Weiss JN**, **Qu Z.** Linking flickering to waves and whole-cell oscillations in a mitochondrial network model. *Biophys J* 101: 2102–2111, 2011. doi:10.1016/j.bpj.2011.09.038.
143. **Korshunov SS**, **Korkina OV**, **Ruuge EK**, **Skulachev VP**, **Starkov AA.** Fatty acids as natural uncouplers preventing generation of O2.$^-$ and $H_2O_2$ by mitochondria in the resting state. *FEBS Lett* 435: 215–218, 1998. doi:10.1016/s0014-5793(98)01073-4.
144. **Komlodi T**, **Geibl FF**, **Sassani M**, **Ambrus A**, **Tretter L.** Membrane potential and delta pH dependency of reverse electron transport-associated hydrogen peroxide production in brain and heart mitochondria. *J Bioenerg Biomembr* 50: 355–365, 2018. doi:10.1007/s10863-018-9766-8.
145. **Lambert AJ**, **Brand MD.** Superoxide production by NADH: ubiquinone oxidoreductase (complex I) depends on the pH gradient across the mitochondrial inner membrane. *Biochem J* 382: 511–517, 2004. doi:10.1042/BJ20040485.
146. **Paterson AW**, **Curtis JC**, **MacLeod NK.** Complex I specific increase in superoxide formation and respiration rate by PrP-null mouse brain mitochondria. *J Neurochem* 105: 177–191, 2008. doi:10.1111/j.1471-4159.2007.05123.x.
147. **Speakman JR**, **Talbot DA**, **Selman C**, **Snart S**, **McLaren JS**, **Redman P**, **Krol E**, **Jackson DM**, **Johnson MS**, **Brand MD.** Uncoupled and surviving: individual mice with high metabolism have greater mitochondrial uncoupling and live longer. *Aging Cell* 3: 87–95, 2004. doi:10.1111/j.1474-9728.2004.00097.x.
148. **Hill BG**, **Benavides GA**, **Lancaster JR Jr**, **Ballinger S**, **Dell'Italia L**, **Jianhua Z**, **Darley-Usmar VM.** Integration of cellular bioenergetics with mitochondrial quality control and autophagy. *Biol Chem* 393: 1485–1512, 2012. doi:10.1515/hsz-2012-0198.
149. **Stepanova A**, **Konrad C**, **Manfredi G**, **Springett R**, **Ten V**, **Galkin A.** The dependence of brain mitochondria reactive oxygen species production on oxygen level is linear, except when inhibited by antimycin A. *J Neurochem* 148: 731–745, 2019. doi:10.1111/jnc.14654.
150. **Miwa S**, **Treumann A**, **Bell A**, **Vistoli G**, **Nelson G**, **Hay S**, **von Zglinicki T.** Carboxylesterase converts Amplex red to resorufin: implications for mitochondrial $H_2O_2$ release assays. *Free Radic Biol Med* 90: 173–183, 2016. doi:10.1016/j.freeradbiomed.2015.11.011.
151. **Chen R**, **Lai UH**, **Zhu L**, **Singh A**, **Ahmed M**, **Forsyth NR.** Reactive oxygen species formation in the brain at different oxygen levels: the role of hypoxia inducible factors. *Front Cell Dev Biol* 6: 132, 2018. doi:10.3389/fcell.2018.00132.
152. **Hoffman DL**, **Brookes PS.** Oxygen sensitivity of mitochondrial reactive oxygen species generation depends on metabolic conditions. *J Biol Chem* 284: 16236–16245, 2009. doi:10.1074/jbc.M809512200.
153. **Antunes F**, **Salvador A**, **Marinho HS**, **Alves R**, **Pinto RE.** Lipid peroxidation in mitochondrial inner membranes. I. An integrative kinetic model. *Free Radic Biol Med* 21: 917–943, 1996. doi:10.1016/s0891-5849(96)00185-2.
154. **Kowald A**, **Hamann A**, **Zintel S**, **Ullrich S**, **Klipp E**, **Osiewacz HD.** A systems biological analysis links ROS metabolism to mitochondrial protein quality control. *Mech Ageing Dev* 133: 331–337, 2012. doi:10.1016/j.mad.2012.03.008.
155. **Li Y**, **Periwal V.** Synergy in free radical generation is blunted by high-fat diet induced alterations in skeletal muscle mitochondrial metabolism. *Biophys J* 104: 1127–1141, 2013. doi:10.1016/j.bpj.2013.01.025.
156. **Toglia P**, **Cheung KH**, **Mak DO**, **Ullah G.** Impaired mitochondrial function due to familial Alzheimer's disease-causing presenilins mutants via $Ca^{2+}$ disruptions. *Cell Calcium* 59: 240–250, 2016. doi:10.1016/j.ceca.2016.02.013.
157. **Li Q**, **Su D**, **O'Rourke B**, **Pogwizd SM**, **Zhou L.** Mitochondria-derived ROS bursts disturb Ca(2)(+) cycling and induce abnormal automaticity in guinea pig cardiomyocytes: a theoretical study. *Am J Physiol Heart Circ Physiol* 308: H623–H636, 2015. doi:10.1152/ajpheart.00493.2014.
158. **Schleicher J**, **Dahmen U.** Computational modeling of oxidative stress in fatty livers elucidates the underlying mechanism of the increased susceptibility to ischemia/reperfusion injury. *Comput Struct Biotechnol J* 16: 511–522, 2018. doi:10.1016/j.csbj.2018.10.013.
159. **Chenna S**, **Prehn JH**, **Connolly NM.** Phenomenological equations for electron transport chain-mediated reactive oxygen species metabolism. In: *2021 IEEE International Conference on Bioinformatics and Biomedicine (BIBM)*. New York: IEEE, 2021, p. 653–658. doi:10.1109/BIBM52615.2021.9669351.
160. **Beard DA.** A biophysical model of the mitochondrial respiratory system and oxidative phosphorylation. *PLoS Comput Biol* 1: e36, 2005. doi:10.1371/journal.pcbi.0010036.
161. **Theurey P**, **Connolly NMC**, **Fortunati I**, **Basso E**, **Lauwen S**, **Ferrante C**, **Moreira Pinho C**, **Joselin A**, **Gioran A**, **Bano D**, **Park DS**, **Ankarcrona M**, **Pizzo P**, **Prehn JHM.** Systems biology identifies preserved integrity but impaired metabolism of mitochondria due to a glycolytic defect in Alzheimer's disease neurons. *Aging Cell* 18: e12924, 2019. doi:10.1111/acel.12924.